



# UNIVERSITÀ DI PARMA

## ARCHIVIO DELLA RICERCA

University of Parma Research Repository

A record of the Messinian salinity crisis in the eastern Ionian tectonically active domain (Greece, eastern Mediterranean)

This is a pre print version of the following article:

*Original*

A record of the Messinian salinity crisis in the eastern Ionian tectonically active domain (Greece, eastern Mediterranean) / Karakitsios, Vasileios; Roveri, Marco; Lugli, Stefano; Manzi, Vinicio; Gennari, Rocco; Antonarakou, Assimina; Triantaphyllou, Maria; Agiadi, Konstantina; Kontakiotis, George; Kafousia, Nefeli; de Rafelis, Marc. - In: BASIN RESEARCH. - ISSN 0950-091X. - 29:(2017), pp. 203-233. [10.1111/bre.12173]

*Availability:*

This version is available at: 11381/2809803 since: 2021-10-07T14:10:28Z

*Publisher:*

Blackwell Publishing Ltd

*Published*

DOI:10.1111/bre.12173

*Terms of use:*

Anyone can freely access the full text of works made available as "Open Access". Works made available

*Publisher copyright*

note finali coverpage

(Article begins on next page)



**A record of the Messinian Salinity Crisis in the eastern Ionian tectonically-active domain (Greece, eastern Mediterranean)**

Journal:	<i>Basin Research</i>
Manuscript ID:	BRE-038-2015
Manuscript Type:	Original Article
Date Submitted by the Author:	18-Mar-2015
Complete List of Authors:	<p>Karakitsios, Vasileios; National and Kapodistrian University of Athens, Department of Historical Geology and Paleontology, Faculty of Geology and Geoenvironment</p> <p>Roveri, Marco; Parma University, Scienze della Terra; Alpine Laboratory of Palaeomagnetism,</p> <p>Lugli, Stefano; University of Modena-Reggio Emilia, Dipartimento di Scienze della Terra</p> <p>Manzi, Vinicio; Università degli Studi di Parma, Dipartimento di Fisica e Scienze della Terra; Alpine Laboratory of Palaeomagnetism,</p> <p>Gennari, Rocco; Università degli Studi di Parma, Dipartimento di Fisica e Scienze della Terra; Alpine Laboratory of Palaeomagnetism,</p> <p>Antonarakou, Assimina; National and Kapodistrian University of Athens, Department of Historical Geology and Paleontology, Faculty of Geology and Geoenvironment</p> <p>Triantaphyllou, Maria; National and Kapodistrian University of Athens, Department of Historical Geology and Paleontology, Faculty of Geology and Geoenvironment</p> <p>Agiadi, Konstantina; National and Kapodistrian University of Athens, Department of Historical Geology and Paleontology, Faculty of Geology and Geoenvironment</p> <p>Kontakiotis, George; National and Kapodistrian University of Athens, Department of Historical Geology and Paleontology, Faculty of Geology and Geoenvironment</p> <p>Kafousia, Nefeli; National and Kapodistrian University of Athens, Department of Historical Geology and Paleontology, Faculty of Geology and Geoenvironment</p> <p>De Rafelis, Marc; Université Pierre et Marie Curie, Institut des Sciences de la Terre</p>
Keywords:	foreland basins, gypsum, evaporites, Zakynthos, paleogeography

1  
2  
3  
4  
5  
6  
7  
8  
9  
10  
11  
12  
13  
14  
15  
16  
17  
18  
19  
20  
21  
22  
23  
24  
25  
26  
27  
28  
29  
30  
31  
32  
33  
34  
35  
36  
37  
38  
39  
40  
41  
42  
43  
44  
45  
46  
47  
48  
49  
50  
51  
52  
53  
54  
55  
56  
57  
58  
59  
60

**A record of the Messinian Salinity Crisis in the eastern Ionian tectonically-active domain (Greece, eastern Mediterranean)**

Vasileios Karakitsios<sup>1\*</sup>

Marco Roveri<sup>2,3</sup>

Stefano Lugli<sup>4</sup>

Vinicio Manzi<sup>2,3</sup>

Rocco Gennari<sup>2,3</sup>

Assimina Antonarakou<sup>1</sup>

Maria Triantaphyllou<sup>1</sup>

Konstantina Agiadi<sup>1</sup>

George Kontakiotis<sup>1</sup>

Nefeli Kafousia<sup>1</sup>

Marc de Rafelis<sup>4</sup>

<sup>1</sup> *National and Kapodistrian University of Athens, Faculty of Geology and Geoenvironment, Department of Historical Geology - Paleontology, vkarak@geol.uoa.gr, aantonar@geol.uoa.gr, kagiadi@geol.uoa.gr, gkontak@geol.uoa.gr, nkafousia@geol.uoa.gr, mtriant@geol.uoa.gr*

<sup>2</sup> *Dipartimento di Fisica e Scienze della Terra, Università degli Studi di Parma, Italy, marco.roveri@unipr.it, vinicio.manzi@unipr.it, rocco.gennari@unipr.it*

<sup>3</sup> *ALP, Alpine Laboratory of Palaeomagnetism, Peveragno, CN, Italy*

<sup>4</sup> *Dipartimento di Scienze Chimiche e Geologiche, Università degli Studi di Modena e Reggio Emilia, Modena, Italy, stefano.lugli@unimore.it.*

<sup>5</sup> *Université Pierre et Marie Curie, Institut des Sciences de la Terre de Paris UMR 7193 CNRS-UPMC, 75005, Paris, France, marc.de\_rafelis@upmc.fr*

*\*corresponding author*

**Abstract**

This integrated study of the Messinian-Zanclean deposits on Zakynthos Island (Ionian Sea) reveals the effect of the Messinian salinity crisis (MSC) in a transitional area between the eastern and the western Mediterranean. The proposed paleogeographic model incorporates new paleontologic, sedimentologic, biostratigraphic, paleomagnetic, and geochemical data. In the Kalamaki-Agassi section, the selenite

1  
2  
3  
4  
5  
6  
7  
8  
9  
10  
11  
12  
13  
14  
15  
16  
17  
18  
19  
20  
21  
22  
23  
24  
25  
26  
27  
28  
29  
30  
31  
32  
33  
34  
35  
36  
37  
38  
39  
40  
41  
42  
43  
44  
45  
46  
47  
48  
49  
50  
51  
52  
53  
54  
55  
56  
57  
58  
59  
60

gypsum is assigned to the Primary Lower Gypsum (PLG) unit deposited during the first MSC stage (5.971-5.60 Ma). In the Agios Sostis section, the gypsum is clastic in origin, derived from the dismantlement and resedimentation during the second MSC stage (5.60-5.55 Ma) of PLG deposits formed in a western basin.

In the Kalamaki pre-evaporitic sequence, nine planktonic foraminifer bioevents are recognized. Five planktonic foraminifer bioevents, nine lithological cycles, and ten oxygen isotope stages are identified within the Pliocene Trubi Formation.

Sedimentologic and paleoecologic analysis indicates a shallow water environment, less than 300 m before the onset of evaporite deposition. Oxygen and carbon isotopic analyses in the upper part of the pre-evaporitic sequence provide evidence for increased isotopically-light carbon input from bacterial sulfate reduction, due to increasing stagnation conditions at the beginning of sulfate deposition. Two intervals are distinguished through the paleoenvironmental reconstruction of the pre-evaporitic Messinian in Kalamaki area: a) 6.45-6.122 Ma and b) 6.122-5.97 Ma. Both the planktonic foraminifer and fish assemblages indicate a cooling phase punctuated by hypersalinity episodes at around 6.05 Ma.

Field observations, borehole data, and seismic profiles indicate that the deposition of Messinian gypsum took place in marginal sub-basins, which formed during the late Messinian in the Pre-Apulian foreland basin before the main phase of the tectonic emplacement of the Ionian zone. In this foreland basin, the Neogene formations over the Ionian zone (east of the westernmost Triassic diapir) formed in the wedge-top depozone, while those overlying Pre-Apulian zone correspond to the main foredeep and the foreland ramp to the foredeep. Erosion of PLG evaporites in the forebulge and wedge-top areas, supplied the foreland basin depocenter with gypsum turbidites.

**Keywords**

Gypsum; foreland basin; evaporites; Zakynthos; paleogeography

**1. Introduction**

The Messinian salinity crisis (MSC; Selli, 1954), the greatest Mediterranean paleoenvironmental perturbation, still offers a fascinating story tale, which inspired researchers for more than fifty years. Despite the fact that certain aspects have been investigated to great extent, major questions still remain open regarding the mechanisms operating during this event (see Roveri *et al.*, 2014a). The scope of the

present study is to describe, in detail, the Messinian-Zanclean deposits and their inclusive fauna in Zakynthos Island (Ionian Sea), a pivotal area located at the transition between the eastern and the western Mediterranean. The MSC-associated environmental changes are revealed through high-resolution integrated stratigraphy. Furthermore, a new tectono-sedimentary evolution model is proposed incorporating new paleontologic, sedimentologic, biostratigraphic, paleomagnetic, and geochemical data.

## 2. The Messinian salinity crisis

Since the early Messinian (7.251 Ma), the gradual restriction of the marine connections between the Mediterranean Sea and the Atlantic Ocean was combined with long-term orbital forcing (Hilgen *et al.*, 2007) to significantly alter the paleoenvironmental conditions in the entire basin. A series of events has been recorded as a result: a) a reduction of deep-water ventilation at 7.15 Ma (Kouwenhoven *et al.*, 1999; 2003; 2006; Kouwenhoven and Van der Zwaan, 2006) associated with diatom-rich and opal-rich sediment deposition between 7.15-6.7 Ma, b) a sudden drop in calcareous plankton diversity at 6.7 Ma (Sierro *et al.*, 1999; 2003; Blanc-Valleron *et al.*, 2002), c) the intensification of bottom-water stagnation and stratification (Kouwenhoven *et al.*, 1999; Sierro *et al.*, 1999; Blanc-Valleron *et al.*, 2002; Sierro *et al.*, 2003; Van Assen *et al.*, 2006), d) calcareous sediment precipitation between 6.3-5.97 Ma, and e) the complete disappearance of planktonic foraminifers during summer insolation minima (Sierro *et al.*, 1999; Bellanca *et al.*, 2001; Blanc-Valleron *et al.*, 2002; Sierro *et al.*, 2003; Manzi *et al.*, 2007; 2011; 2013; Gennari *et al.*, 2013).

According to the three-step model for the development of the salinity crisis proposed by Roveri *et al.* (2008a; 2014a), the MSC Stage 1 commenced synchronously at 5.97 Ma throughout the Mediterranean basin (Krijgsman *et al.*, 1999a; 2002; Manzi *et al.*, 2013). It is recorded by evaporite deposition, the Primary Lower Gypsum (PLG), in the marginal areas (including basins with water depth less than 200 m) and by evaporite-free dolomites and organic-rich shales, in the intermediate and deeper basins (Manzi *et al.*, 2007; 2011; De Lange and Krijgsman, 2010; Dela Pierre *et al.*, 2012). The deposition of gypsum took place subaqueously, in shallow water settings with moderate oxygenation (Lugli *et al.*, 2010). The deposition of up to 16 precession-induced gypsum-marl cycles comprising PLG continued until ~5.6 Ma

1  
2  
3  
4  
5  
6  
7  
8  
9  
10  
11  
12  
13  
14  
15  
16  
17  
18  
19  
20  
21  
22  
23  
24  
25  
26  
27  
28  
29  
30  
31  
32  
33  
34  
35  
36  
37  
38  
39  
40  
41  
42  
43  
44  
45  
46  
47  
48  
49  
50  
51  
52  
53  
54  
55  
56  
57  
58  
59  
60

(Vai 1997; Krijgsman *et al.*, 1999b; Hilgen *et al.*, 2007; Lugli *et al.*, 2010), and was concluded by a major subaerial exposure event creating the Messinian Erosional Surface (MES) in the marginal basins.

During MSC stage 2 (5.6 – 5.55 Ma; Roveri *et al.*, 2014a), the Messinian Erosional Surface (MES) developed across the Mediterranean margins due to subaerial erosion. Two intense glacial periods (TG14 and TG12) further limited fresh-water input and probably stopped the outflow of Mediterranean water to the Atlantic (Meijer and Krijgsman, 2005; Hilgen *et al.*, 2007; Roveri *et al.*, 2014a). Primary halite occasionally precipitated in the marginal basins (Manzi *et al.*, 2012) as well as in the sub-basins (Lugli *et al.*, 1999). In the margins, tectonic activity, in conjunction with general slope instability, led to the erosion and resedimentation of the PLG and the widespread deposition of clastic evaporites (Resedimented Lower Gypsum; RLG *sensu* Roveri *et al.*, 2008b) throughout the Mediterranean (Ricci Lucchi, 1973; Robertson *et al.*, 1995; Kontopoulos *et al.*, 1997; Fortuin and Krijgsman, 2003; Roveri *et al.*, 2003; Manzi *et al.*, 2005; Roveri and Manzi, 2006; Manzi *et al.*, 2011; Omodeo-Salé *et al.*, 2012; Lugli *et al.*, 2013; Roveri *et al.*, 2014a; Manzi *et al.*, 2015). On Sicily, RLG deposited in adjacent depocenters as a result of tectonic activity (Butler *et al.*, 1995; Roveri *et al.*, 2008a; Manzi *et al.*, 2011) and is associated with hydrocarbon migration (Iadanza *et al.*, 2013).

The MSC stage 3 (5.55 – 5.33 Ma; Manzi *et al.*, 2009; Roveri *et al.*, 2014a) was characterized by selenite and cumulate gypsum precipitation in the shallow-water sub-basins of Sicily and Cyprus (Rouchy, 1982; Roveri *et al.*, 2008a; Manzi *et al.*, 2009; 2015); mostly clastic sediments were deposited in the northern and western Mediterranean. Typical of this stage is the Lago-Mare facies (Gignoux, 1936; Ruggieri, 1967; Orszag-Sperber, 2006), brackish to fresh-water sediments with Paratethyan fauna, indicating surface-water dilution which may have been locally interrupted by evaporitic events (Upper Gypsum; UG; Manzi *et al.*, 2009). The most widely accepted scenario so far hypothesizes a complete isolation of the Mediterranean from the Atlantic, with occasional connection to the Paratethys (Orszag-Sperber, 2006; Rouchy & Caruso, 2006; Roveri *et al.*, 2008b). However, the fossil fish record of northern Italy (Carnevale *et al.*, 2006; 2008), as well as biomarker evidence (Mezger, 2012), suggests that the Mediterranean retained its connection to the Atlantic, although maybe not continuously (Roveri *et al.*, 2014a,b,c).

The end of the MSC and the return to fully marine conditions is considered to have taken place at 5.33 Ma through a catastrophic event, flooding the entire Mediterranean basin (Hsu *et al.*, 1973; Blanc-Valleron, 2002; Meijer & Krijgsman, 2005; Garcia-Castellanos *et al.*, 2009). Lithologic and paleontologic observations generally concur to this hypothesis. The Messinian/Zanclean boundary commonly includes a transitional interval, rich in organic matter (Roveri *et al.*, 1998; 2008b; Gennari *et al.*, 2008), and it is followed by the typical early Pliocene marine deposits of the ‘Trubi’ or ‘Argille Azzurre’ Formations.

### 3. Geological setting

The Zakynthos Island’s alpine sequence belongs (Fig. 1) to the Pre-Apulian and partly to the Ionian zone – separated by the Ionian thrust – whose emplacement took place during the early Pliocene (BP, 1971; Sorel, 1976; Nikolaou, 1986; Underhill, 1989, Karakitsios & Rigakis, 2007). The Pre-Apulian zone of Zakynthos comprises Upper Cretaceous to Pleistocene sediments, while the Ionian zone is represented by Triassic breccias and microcrystalline gypsum corresponding to the lower stratigraphic unit of this zone. Cretaceous to Oligocene carbonates outcrop on Marathonisi Islet (2.5 km east of Keri; Fig. 1) and probably represent a transitional facies between the Ionian and Pre-Apulian domains (Nikolaou, 1986). Numerous reverse faults cut the Pre-Apulian sequence along the NW-SE direction, exposing late Miocene sandstones and marls along the coastal sections between Agios Sostis and Keri (Fig. 1); these are significantly folded, indicating a post-Miocene age for the Ionian thrust emplacement (Underhill, 1989; Karakitsios, 2013).

The Ionian sequence is unconformably overlain by Neogene and Quaternary deposits outcropping mainly in southeastern Zakynthos. These are similar to those of the Pre-Apulian zone, but thinner and characterized by unconformities (Dermitzakis, 1977; Nikolaou, 1986), and they consist of early Miocene clastic sediments outcropping in the Skopos area, followed by late Messinian marls and shales (30-100 m thick) intercalated by gypsum (Fabricius *et al.*, 1998). The early Pliocene deposits include calcareous pelagic marls (Trubi limestone) and sandstone intercalations (Kontopoulos *et al.*, 1997). The late Pliocene to Pleistocene deposits comprise a transgressive clastic sequence recording sea-level changes concurrent with intense tectonic movements (Triantaphyllou, 1996; Triantaphyllou *et al.*, 1997; Duermeijer *et al.*, 1999; Zelilidis *et al.*, 1998; Agiadi *et al.*, 2010; Papanikolaou *et al.*, 2011).



1  
2  
3  
4  
5  
6  
7  
8  
9  
10  
11  
12  
13  
14  
15  
16  
17  
18  
19  
20  
21  
22  
23  
24  
25  
26  
27  
28  
29  
30  
31  
32  
33  
34  
35  
36  
37  
38  
39  
40  
41  
42  
43  
44  
45  
46  
47  
48  
49  
50  
51  
52  
53  
54  
55  
56  
57  
58  
59  
60

**4. Methods**

**4.1 Field geology, borehole, and seismic data**

Field observations were combined with detailed sampling along the Kalamaki-Argassi and Agios Sostis areas, in the south-eastern part of Zakynthos Island. A main concern was to distinguish the Ionian zone Triassic gypsum (Karakitsios, 1995) from the Messinian gypsum, both expressed in this area. The Ionian thrust’s cartographic position and the Neogene deposits’ distribution were based on new tectonic, stratigraphic, and sedimentologic observations, in conjunction with a reinterpretation of the available boreholes and onshore seismic data.

**4.2 Planktonic Foraminifera**

In the Kalamaki and Agios Sostis sections, 198 samples were collected. In the Kalamaki section, 175 samples were obtained at 0.05 to 0.50-meter intervals in the west (pre-MSC) and the east subsection (Messinian-Zanclean), representing 37.1 m of sediment thickness. In the Agios Sostis section (Fig. 7), 23 samples were collected at 0.05 to 1-meter intervals for a total thickness of 20 m. A total of 14 samples (AS 1-14) were studied from the 16.5 m of the pre-evaporitic sequence (sampling step about 0.30 to 1 m), and nine samples were examined from the 20 m of the post-evaporitic sequence. Three samples (AS 15-17) were obtained from the first 1.20 m of the post-evaporitic sequence, which are rich in gypsum crystals, six samples (AS 18-23) were taken from the last 1.5 m of the Agios Sostis section.

The samples were washed through a 63-μm sieve. Biostratigraphy is based on the semi-quantitative analysis of planktonic foraminifers. The bioevents considered in this study were based on the changes in the planktonic foraminiferal assemblage observed in the fraction larger than 125 μm. The recognition of zonal boundaries was based on the biozonal scheme of Iaccarino *et al.* (2007) and through correlation to the astronomically calibrated succession of the Mediterranean area (Krijgsman *et al.*, 1999b; Sierro *et al.*, 2001; Iaccarino *et al.*, 1999; Gennari *et al.*, 2008).

The planktonic foraminifer paleoecological remarks are based on the quantitative abundance distribution of the species, identified in the section, and their modern ecological affinities (Bè & Tolderlund, 1971; Hemleben *et al.*, 1989).

**4.3 Calcareous nannofossils**

Smear slides were prepared following the standard technique described by Perch Nielsen (1985) and Bown & Young (1998). The taxonomy of the determined calcareous nannofossil species was in accordance with Aubry (1984, 1988, 1989, 1990, and 1999) and Perch-Nielsen (1985). Biostratigraphic analysis was based on the standard biozonal scheme of Martini (1971). Biochronology and the numerical ages of the biozone boundaries were assigned according to Lourens *et al.* (2004), Raffi *et al.* (2006), and Backman *et al.* (2012).

Nannofossil biostratigraphy incorporated qualitative and semiquantitative analyses. Qualitative methods are traditionally based on the estimation of index-species presences, obtained through a rough scan of the sample. Concerning semiquantitative methods, these were mainly used to overcome the very terrigenous and relatively shallow nature of the studied samples, in which nannofossils are rather scarce. To obtain accurate biostratigraphic estimations, up to 100 fields of view were investigated per slide, using a Leica DMLSP optical polarizing light microscope at 1250x magnification. Semiquantitative abundances of the identified taxa were categorized as follows: A. abundant, more than one specimen in every field of view; C. common, one specimen in every ten fields of view; R. rare, one specimen in every 50 fields of view; P. present, one specimen in more than 100 fields of view; and RW. reworked specimens.

The biostratigraphic framework for the Trubi deposits was based on the paleoecological affinities of the following calcareous nannofossil species. Small *Gephyrocapsa* spp. <3  $\mu$  m, are considered upper photic-zone opportunistic taxa, indicating eutrophic conditions (e.g., Flores *et al.*, 2005). Discoasterids, generally preferring warm and oligotrophic waters, are lower photic-zone inhabitants, which increase their abundance with deep pycnocline (Flores *et al.*, 2005). *Helicosphaera carteri* is commonly found in warm waters (e.g., Baumann *et al.*, 2005), associated with moderately-elevated nutrient levels (e.g., Ziveri *et al.*, 2004). It is commonly accepted as a species tolerant of low salinities and high terrigenous input (Triantaphyllou *et al.*, 2009a,b); it is highly frequent in regions influenced by riverine discharge (e.g., Cros, 2001), as a coastal-water taxon (e.g., Dimiza *et al.*, 2014). In addition, Rhabdosphaeraceae prefer warm and oligotrophic waters (Triantaphyllou *et al.*, 2004; Dimiza *et al.*, 2008; Malinverno *et al.*, 2009) and *Scyphosphaera* spp. are common in tropical-subtropical regions (Rade, 1975).

1  
2  
3  
4  
5  
6  
7  
8  
9  
10  
11  
12  
13  
14  
15  
16  
17  
18  
19  
20  
21  
22  
23  
24  
25  
26  
27  
28  
29  
30  
31  
32  
33  
34  
35  
36  
37  
38  
39  
40  
41  
42  
43  
44  
45  
46  
47  
48  
49  
50  
51  
52  
53  
54  
55  
56  
57  
58  
59  
60

**4.4 Fish otoliths**

The same samples collected for the biostratigraphic analysis were also examined for the fish otolith content. In addition, several 25 kg bulk samples were obtained throughout the pre-evaporitic interval and the upper part (Trubi Formation) of Kalamaki section, as well as from each of the marl beds alternating with the gypsum (Fig. 2). The purpose was to identify the fish fauna in the area before, during, and after the MSC; to determine the timing of the reestablishment of a purely marine fauna after the crisis (Carnevale *et al.*, 2006); and to estimate the paleoenvironmental conditions especially just before the onset of evaporite deposition. Fish otoliths were described according to the criteria set by Nolf (1985) and systematically identified based on the scheme of Nelson (2006). The methodology of Nolf & Brzobohaty (1994), as readjusted by Agiadi *et al.*, (2010), was applied to estimate the paleodepth. The paleoecological analysis was based on the fish’s present-day distribution and ecological data acquired through the FishBase database (Froese & Pauly, 2014).

**4.5 Magnetostratigraphy**

The magnetostratigraphy of the Kalamaki section is based on a subset of the same samples used for biostratigraphy, 61 samples in total (Fig. 2). Core samples were obtained with a water-cooled diamond-head corer installed on an electric driller. The standard specimens were thermally demagnetized in an ASC hoven and the natural remanent magnetization (NRM) was measured on a 2G-Enterprises DC SQUIDS cryogenic magnetometer, in a magnetically shielded room at the ALP Laboratory of Peveragno (Italy). Samples were first heated to 90°C, and, then, successive 30°C steps were applied up to a maximum of 560°C. The magnetic susceptibility was monitored during heating to detect mineralogical changes. The NRM dataset was processed using the Remasoft software (Chadima & Hrouda, 2006) to calculate the direction of the characteristic remanent magnetization (ChRM) and the Virtual Geomagnetic Pole (VGP) for each sample.

**4.6 Oxygen and carbon stable isotopes**

The isotopic composition of bulk sediments and planktonic foraminifers focused on investigating the degree of evaporation before the commencement of evaporite deposition, as well as the system inertia after the MSC. The oxygen and carbon

isotopic compositions were measured on both the bulk sediment (late Miocene deposits;  $\delta^{18}\text{O}_{\text{carb}}$ ,  $\delta^{13}\text{C}_{\text{carb}}$ ) as well as on the planktonic foraminifers *Turborotalita multiloba*, *Orbulina universa* (late Miocene;  $\delta^{18}\text{O}_{\text{foram}}$ ,  $\delta^{13}\text{C}_{\text{foram}}$ ) and *Globigerinoides obliquus* (Pliocene; Trubi Formation;  $\delta^{18}\text{O}_{G.\text{obliquus}}$ ,  $\delta^{13}\text{C}_{G.\text{obliquus}}$ ), using a mass spectrometer VG SIRA 9 and a KIEL-IV carbonate device coupled online to a Delta V Advantage IRMS (Thermo Scientific), respectively. The  $\text{CO}_2$  extraction was attained through reaction of powder samples (50-100 mg) with anhydrous orthophosphoric acid, at 50°C. The values were expressed in per mil relative to the Vienna PDB (V-PDB) standard reference. Long-term analytical precision reached  $\pm 0.1\text{‰}$  for  $\delta^{18}\text{O}_{\text{carb}}$ ,  $\pm 0.05\text{‰}$  for  $\delta^{13}\text{C}_{\text{carb}}$ ,  $\pm 0.08\text{‰}$  for  $\delta^{18}\text{O}_{\text{foram}}$  and  $\delta^{18}\text{O}_{G.\text{obliquus}}$ , and  $\pm 0.05\text{‰}$  for  $\delta^{13}\text{C}_{\text{foram}}$  and  $\delta^{13}\text{C}_{G.\text{obliquus}}$ .

#### 4.7 Strontium isotopes

Two gypsum samples (Fig. 2) were analyzed for strontium isotope content in order to distinguish the stage 1 PLG deposits from the stage 3 UG (Flecker *et al.*, 2002; Roveri *et al.*, 2014b). Strontium isotope analyses were carried out at the Scottish Universities Environmental Research Centre in East Kilbride, Scotland (SUERC). Samples were leached in 1M ammonium acetate prior to acid digestion with  $\text{HNO}_3$ . Strontium was separated using Eichrom Sr Spec resin. Matrix elements were eluted in 8M  $\text{HNO}_3$  and 3M  $\text{HNO}_3$ , before elution of Sr in 0.01M  $\text{HNO}_3$ . Total procedure blank for Sr samples prepared using this method was b200 pg. In preparation for mass spectrometry, Sr samples were loaded onto single Re filaments with a Ta-activator similar to that described by Birck (1986). Sr samples were analyzed with a VG Sector 54-30 multiple collector mass spectrometer. A  $^{88}\text{Sr}$  intensity of 1V ( $1\text{Å} \sim 10 - 11\text{A}$ )  $\pm 10\%$  was maintained. The  $^{87}\text{Sr}/^{86}\text{Sr}$  ratio was corrected for mass fractionation using  $^{86}\text{Sr}/^{88}\text{Sr} = 0.1194$  and an exponential law. The mass spectrometer was operated in the peak-jumping mode, with data collected as 15 blocks of 10 ratios providing an internal uncertainty of b0.000020 (2 S.E.). For this instrument NIST SRM 987 gave  $0.710249 \pm 0.000008$  (1 S.D.,  $n = 17$ ) during the course of the present study.

## 5. Results

### 5.1 Field observations

#### 5.1.1 Kalamaki–Argassi area

1  
2  
3  
4  
5  
6  
7  
8  
9  
10  
11  
12  
13  
14  
15  
16  
17  
18  
19  
20  
21  
22  
23  
24  
25  
26  
27  
28  
29  
30  
31  
32  
33  
34  
35  
36  
37  
38  
39  
40  
41  
42  
43  
44  
45  
46  
47  
48  
49  
50  
51  
52  
53  
54  
55  
56  
57  
58  
59  
60

The Neogene sequence of the Kalamaki-Argassi area lies unconformably over the Ionian zone basement. The following stratigraphic units are recognized (Fig. 2):

Pre-evaporitic unit

The lower 14.5 m of the succession consist of alternating massive and laminated marls with rare calcareous-marl and calcarenite intercalations. From 5 to 13 m, bivalves, *Discospirina*, pteropods, echinoids, and molluscs are observed. Between 14.5 to 17.5 m, some slumps and chaotic horizons occur. The rest of the pre-evaporitic sequence is partially covered by Quaternary detritus (Fig. 3a).

Evaporitic unit

The previous unit is followed in stratigraphic continuity by a 108 m-thick evaporite succession (Figs. 2 and 4). Eight gypsum-marl cycles are identified (A to H), exhibiting different gypsum depositional facies: massive, massive stratified, banded, laminite, and branching selenite (Lugli *et al.*, 2010); thin gypsrudite and gypsarenite intercalations appear in the upper one-third of the succession (Fig. 3c,d,e,f, and 4). Based on these evaporitic facies and on the conformable superposition on the pre-MSC succession, these deposits can be ascribed to the Primary Lower Gypsum unit (PLG; Roveri *et al.*, 2008a) accumulated during the MSC stage 1 (5.971-5.60; CIESM, 2008; Manzi *et al.*, 2013). The uppermost eight meters of the gypsum succession are clastic deposits, comprising laminated greenish marls; interrupted, after the fourth meter of the succession, by a dm-thick gypsarenite bed (cycle H of depositional gypsum type; Fig. 2). These sediments originate from the hanging wall of a small normal fault separating the lower from the uppermost part of the succession.

Post-evaporitic unit

The uppermost part of the gypsum unit is capped by an angular unconformity (Fig. 3b) that can be correlated with the MES (CIESM, 2008; Roveri *et al.*, 2014a). The unconformity is sealed by a four m-thick unit consisting of alternating greenish and discontinuous calcareous marl beds that can be assigned to the uppermost Messinian Lago-Mare 3b). This unit in turn is sharply overlain by the Trubi Formation, which begins with three meters of whitish massive marly limestones, overlain by an alternation of decametric marly limestones and laminated marl beds. The Trubi Formation can be subdivided into nine lithological cycles (Figs. 3b and 5). In the Argassi area (Fig. 1), the PLG is well-recorded (Fig. 8a,b), and it comprises eight gypsum-marl cycles that can be correlated with those of the Kalamaki section (Fig. 6). However, in Argassi area, it is not possible to observe the stratigraphic

transition of the evaporitic succession to the overlying and the underlying formations, due to tectonics and the Quaternary debris cover.

#### 5.1.2 Agios Sostis area

The Neogene succession of Agios Sostis area lies over the Pre-Apulian zone sequence. The following stratigraphic units are recognized:

##### Pre-evaporitic unit

In the Agios Sostis section, the lowermost part of this unit consist of decameter-thick shale and sandstone alternations, exhibiting upward decrease in clastic input (Figs. 7 and 8c). These deposits are overlain by 3.5 m of thin sandstone beds with marl intercalations, which in turn are capped by 3 m of laminated green shale and marl alternations.

##### Evaporitic unit

In the Agios Sostis area, two parallel linear gypsum outcrops are observed, the Ploumari outcrop and the Panagia (Machairado) outcrop (Fig. 1). The western outcrop (Ploumari) consists of primary bottom-growth selenite (PLG) deposited in shallow-water settings (less than 200 m; Lugli *et al.*, 2010) and is exposed for about three km. The PLG succession is here incomplete and represented only by one or two gypsum beds consisting of very large crystals that are typically found in the two lowermost PLG cycles (Lugli *et al.*, 2010).

Conversely, the eastern outcrop (Panagia) exposes mainly clastic gypsum deposits that derive from the resedimentation of older PLG deposits. Moving from Panagia to Agios Sostis, in a NNW-SSE direction (Fig. 1), it is possible to observe a down-slope transition of different gravity-flow deposits: from chaotic deposits including dm-thick resedimented gypsum blocks to gypsum turbidites alternated with primary gypsum cumulate. These deposits are well exposed in the Agios Sostis section.

This suite of evaporite-bearing gravity-flow deposits suggests that the Panagia sediments derived from the erosion of PLG located to the west, like those outcropping in Ploumari. Unfortunately, the basal contact of the evaporitic unit is not visible in this sector. Thus, it cannot be excluded that the PLG deposits are actually blocks slit downslope from a more western position; e.g., from the backbulge basin on top of the Apulian terrains. Westward, these PLG deposits were completely eroded during the late Messinian, as indicated by the angular unconformity between the early Pliocene conglomerates - sandstones and the early-middle Miocene marls, which was first

1  
2  
3  
4  
5  
6  
7  
8  
9  
10  
11  
12  
13  
14  
15  
16  
17  
18  
19  
20  
21  
22  
23  
24  
25  
26  
27  
28  
29  
30  
31  
32  
33  
34  
35  
36  
37  
38  
39  
40  
41  
42  
43  
44  
45  
46  
47  
48  
49  
50  
51  
52  
53  
54  
55  
56  
57  
58  
59  
60

observed by Nikolaou (1986) in the Perlakia area (about one km north of the Keri village; Fig. 1).

Along the Agios Sostis shoreline, a 16 m-thick gypsum unit lies above an erosional surface developed on top of the pre-evaporitic succession (Fig. 7 and 8c). It consists of several alternations of primary (cumulate) and clastic gypsum (gypsrudite, gypsarenite, and gypsiltite; Figs. 7 and 8d, f), commonly showing high-angle cross- and convolute lamination (Figs. 7 and 8e). This succession is mostly characterized by clastic gypsum deposits and lacks the *in situ* shallow-water selenite described in the Kalamaki–Argassi area. This evaporitic unit derives from the dismantlement and resedimentation of PLG deposits and, thus, can be ascribed to the RLG unit, deposited during the stage 2 of the salinity crisis (5.60-5.55; CIESM, 2008; Roveri *et al.*, 2008a). The entire RLG unit shows an upward increase of the siliciclastic component and is divided into four units, each topped by a centimetric marly bed. Approximately two meters of hybrid sandstones are capping the clastic evaporite unit. The urban fabric of Agios Sostis Community (harbour) does not allow further observations. Nevertheless, the section’s continuity is observed in the Agios Sostis islet (Fig. 1), which is separated from the main coastal section by a fault; the two sections are located approximately 130 m apart. In this islet, about eleven meters of interbedded graded sandstones and marls are observed (level 6 of Fig. 7), exhibiting an upward decrease in siliciclastic material. At approximately 37-38 m above the base of the Agios Sostis composite section, a normal fault with a throw of about two meters is observed (lower level 6 of Fig. 7). The last seven meters of the section (levels 46-53 m) are well observed in the rocky elevation of the Agios Sostis harbor, some 130 meters NNW of the islet (upper level 6 and level 7 of Fig. 7). They comprise a six m-thick succession of graded sandstone and marl alternations, followed by 1.5 m of whitish marls belonging to the post-evaporitic Trubi Formation.

**5.2 Borehole and seismic reflection data**

Correlation of the available borehole logs (Fig. 9) shows that the Neogene deposits (Messinian gypsum included), deposited over the Pre-Apulian basement, increase their thickness east-to-southeastward, following the dipping of the Alikanas monocline. The Neogene sediment thickness ranges from 800 m in the west to 1350 m in the east. This eastward thickening, toward the depocenter of the basin, is confirmed by the Alikanas basin onshore seismic profile (Fig. 10). Furthermore, the

seismic profile suggests that the Ionian thrust is located west of the western Ionian Triassic diapir (Agia Dynati diapir; Fig. 1), more to the west than previously considered. In addition, in the Agios Kyrikos-1 well (Fig. 9; AK1), at the Alikanas basin's depocenter, an increase in the salinity of the drilling mud was recorded, when the drilling penetrated the Messinian evaporites. This fact, combined with the observation of a simultaneous speed reversal of the seismic waves at the same stratigraphic level (C. Nikolaou, personal communication), is an indirect indication of the presence of halite in the Messinian evaporitic unit at the basin's depocenter zone.

### 5.3 Planktonic Foraminifera

#### 5.3.1 Kalamaki section

The abundance of planktonic foraminifers varies throughout the section. In the pre-evaporitic sequence, several samples are barren or contain only benthic foraminifers. The preservation is generally good in the lower part of the section, up to 14 m from the base, and it becomes moderate upward. Planktonic foraminifers within the Trubi Formation are very abundant and preserved well.

##### a) Western subsection

In the pre-evaporitic part of the Kalamaki section (Fig. 2), the following species are identified: *Turborotalita multiloba*, *Turborotalita quinqueloba*, *Globigerinita glutinata*, *Globigerina bulloides*, *Globigerina obesa*, *Orbulina universa*, and *Neogloboquadrina acostaensis* (dextral and sinistral forms). *Turborotalita multiloba* occurs from 0.6 m (sample KAL 5) up to 7.2 m (KAL 41), and it is found together with rare specimens of *Globigerinoides* spp., *O. universa*, and *T. quinqueloba*. In the lowermost two meters of the section (KAL 7 -KAL 10), *T. multiloba* represents the totality of the assemblage, making it monospecific. A paracme interval, within its abundance distribution, is recognized between 1.95-4.3 m (KAL 11-KAL 23), where the species is very rare or absent. The paracme end of this interval (bioevent 3a, fig. 15) is also recognized in Sorbas Basin, in the upper part of cycle UA23, and in Caltanissetta Basin, just above the influx of *G. scitula*. The distribution of *T. multiloba* is similar in Kalamaki and Falconara sections and is probably related to the paleoecological requirements of the species and the basin's configuration during this period. The species becomes the main planktonic foraminifera faunal component up to 7.2 m. Upward, it exhibits two significant peaks at 9 and 10.5 m (KAL 56 and KAL 64) corresponding to its highest abundance.



1  
2  
3  
4  
5  
6  
7  
8  
9  
10  
11  
12  
13  
14  
15  
16  
17  
18  
19  
20  
21  
22  
23  
24  
25  
26  
27  
28  
29  
30  
31  
32  
33  
34  
35  
36  
37  
38  
39  
40  
41  
42  
43  
44  
45  
46  
47  
48  
49  
50  
51  
52  
53  
54  
55  
56  
57  
58  
59  
60

*Turborotalita quinqueloba* and *G. glutinata* are rare in the lower part of the section and dominate the assemblages, in the thick massive marly interval from 7 to 8.5 m (KAL 39 through KAL 49).

*Neogloboquadrina acostaensis* is generally rare in the section, displaying a relative abundance fluctuation between sinistral and dextral specimens. Sinistral forms are more abundant from the base up to 1.5 m (KAL 9), whereas dextral representatives are prevalent in the 2.7 - 8.4 m interval (KAL 15-KAL 49). Sinistral forms prevail again in the interval between 8.8 and 9.2 m (KAL 54-KAL 57; 60-70%) and at 10.5 m (KAL 64; 40%).

*Globorotalia scitula* is present with two short influxes at 3.7 and 9.3 m (KAL 20 and KAL 58), between the two peaks of *T. multiloba*. The upper part of the section, from 10.5 m until just below the slumped interval (KAL 65-89), is characterized by the dominance of *O. universa*, *G. bulloides*, and *G. obesa*, which reach their maximum abundance in sample KAL 89 (14.3 m). Above the slumped interval, planktonic Foraminifera are absent up to sample KAL 105, where few representatives of *N. acostaensis* are present. Benthic foraminifera are very abundant in the samples before the first gypsum.

*b) Central subsection*

The upper part of the PLG succession in the Kalamaki section (gypsum cycle H; Figs. 2, 3b, and 4) is characterized by the sporadic presence of the planktonic foraminifera: *Globoturborotalita nepenthes*, *Globigerinoides*, *G. bulloides*, *Sphaeroidinellopsis* spp., and *O. universa*.

*c) Eastern subsection*

The Lago-Mare unit is characterized by the scattered presence of *Sphaeroidinellopsis* spp., *G. nepenthes*, and *N. acostaensis*. Just below Trubi Formation (KAL 134) the planktonic foraminifer assemblage is well-diversified mainly containing *Sphaeroidinellopsis*, *G. obliquus*, *O. universa*, and *N. acostaensis* dextral specimens.

*d) Trubi Formation*

Planktonic foraminifers become continuously abundant and well preserved from the base of the Trubi Formation upward (Figs. 2, 3b, and 5); they are mainly represented by *Sphaeroidinellopsis* spp., *G. obliquus*, *N. acostaensis* (dextral and sinistral), *Globorotalia margaritae*, *G. bulloides*, and *O. universa*. *Neogloboquadrina acostaensis* sinistral-coiling specimens exhibit an influx in samples KAL 142 and KAL

149. *Sphaeroidinellopsis* spp. show an acme interval from KAL 147 through KAL 160. *Globorotalia margaritae* first commonly occurs in KAL 171.

### 5.3.2 Agios Sostis section

#### a) Pre-evaporitic unit

The samples from the pre-evaporitic sediments of Agios Sostis coastal section are barren of foraminifera. The complete sequence is characterized by the presence of gypsum crystals, possibly of diagenetic origin; gypsum was also recovered from the sieved residual.

#### b) Post-evaporitic unit

The lower 1.2 m of the post-evaporitic sequence, in the coastal elevation of Agios Sostis harbor, are barren of foraminifera, whereas the uppermost 1.5 m contains a rich planktonic fauna. Samples AS 18 and 19 yield specimens of *Globorotalia conomiozea* (Fig. 7). This species disappeared from Mediterranean during the pre-evaporitic phase of the MSC, at 6.52 Ma (Krijgsman *et al.*, 1999; Sierro *et al.*, 2001). Therefore, its presence in the post-evaporitic sequence of Agios Sostis may be assumed due to reworking. The last four samples of the section (AS 20-23), collected one meter below the Trubi Formation, are characterized by the presence of *G. obliquus*, *G. trilobus*, *G. decoraperta*, *G. nepenthes*, *G. bulloides*, *G. falconensis*, *T. quinqueloba*, *Orbulina* sp., *Sphaeroidinellopsis* spp., and *N. acostaensis*.

## 5.4 Calcareous nannoplankton

#### a) Western subsection

The lower part of the Kalamaki sequence (KAL 10-50) features an abundant nannofossil assemblage in good preservation state (Fig. 2). The prevailing species are *Helicosphaera carteri*, *Calcidiscus leptoporus*, *Umbilicosphaera jafari*, and small *Reticulofenestra* spp. (*R. haqii*, *R. minutula*). Six-rayed discoasters are very rare, and *Discoaster quinquerramus* is practically absent. Nearly monospecific assemblages of *Sphenolithus abies* are observed upward. The upper part of the sequence is characterized by the sporadic presence of *Amaurolithus delicatus*, *A. primus*, *A. tricorniculatus*, and rare *Nicklithus amplificus*.

#### b) Central subsection

The upper part of the PLG in Kalamaki section (KAL 114-125; Fig. 2) is characterized by intense reworking and contains rare nannofossil specimens, in bad preservation,

1  
2  
3  
4  
5  
6  
7  
8  
9  
10  
11  
12  
13  
14  
15  
16  
17  
18  
19  
20  
21  
22  
23  
24  
25  
26  
27  
28  
29  
30  
31  
32  
33  
34  
35  
36  
37  
38  
39  
40  
41  
42  
43  
44  
45  
46  
47  
48  
49  
50  
51  
52  
53  
54  
55  
56  
57  
58  
59  
60

mostly reworked assemblages of Oligocene-Miocene age also including Cretaceous taxa.

c) *Eastern subsection*

The Lago-Mare facies unit (KAL 120-134), beneath the Trubi Formation of Kalamaki section (Fig. 2), displays rare to common well-preserved small *Gephyrocapsa* spp. coccoliths (1.5-3.0 µm) within a rich but reworked assemblage. Just below the Trubi Formation (KAL 134), the rare presence of *Ceratolithus acutus* together with specimens of *Reticulofenestra zancleana* is recorded.

**5.5 Fish remains**

Sixteen fish taxa are identified in the pre-evaporitic sediments of Kalamaki section based on the otolith remains (Table 1; Fig. 11). The samples obtained from the marls in between the evaporites, as well as from the upper part of Kalamaki section, including the Trubi Formation, did not yield otolith remains. The Kalamaki pre-evaporitic teleost fauna resembles those identified by Girone *et al.* (2010) in the pre-evaporitic successions of northern Italy. Indeed the great diversity of the benthic-benthopelagic group is asserted here as well. *Gadiculus labiatus* is the most frequent benthic species in the assemblages, although the overall abundance of gobiids is higher. However, the gobiid specimens are very small and indeterminable to the specific, or even generic, level. The pelagic realm is dominated by myctophids, particularly those belonging to the genus *Diaphus*, which is much diversified; five different species are identified, with high abundance in the studied samples. Notably, *Diaphus rubus* and *Myctophum coppa*, two fossil species first reported by Girone *et al.* (2010) in the pre-evaporitic sequence of northern Italy, are also found in pre-evaporitic succession of Kalamaki section (samples KAL 6, KAL 13, KAL 15, KAL 26, KAL 27, KAL 31, KAL 41, KAL 81, KAL 87, KAL 89, KAL 95). In biogeographic terms, six of the fourteen fish, identified at the specific level, are extinct today; the remaining still inhabit the Mediterranean Sea, apart from *Physiculus huloti*, which occurs only in the Atlantic Ocean (Cohen *et al.*, 1990). *Diaphus* cf. *pedemontanus*, *D. rubus*, and *Myctophum coppa* are absent in the so far studied Pliocene and Pleistocene assemblages of the eastern Mediterranean (Agiadi *et al.*, 2010; Agiadi *et al.*, 2013a; Agiadi, 2013). During the time interval preceding the onset of the MSC, the Kalamaki area presents a well-diversified fish fauna, comprising both abundant pelagic and benthic-

benthopelagic fish. The continuous presence of gobiids throughout the basal part of the section and the occurrence of *Buglossidium* sp. in sample *KAL* 31 suggest rather shallow water-depths before the onset of gypsum deposition. In fact, the occurrence of benthopelagic *Physiculus* aff. *huloti* (bulk sample *KAL* base) indicates depths less than 320 m (OBIS, 2006). However, the great diversity and abundance of the genus *Diaphus* and the presence of gadids (*Gadiculus argenteus* and *Gadiculus labiatus*) in the upper part of the basal sequence (just prior to the gypsum deposits, samples *KAL* 27, *KAL* 28, *KAL* 38, *KAL* 39, *KAL* 45), suggest the area was not secluded, and depths certainly greater than 50 m may be expected. In addition, *Maurolicus muelleri* is present in almost all the samples examined and in great abundances. Although this bathypelagic species has a large bathymetric distribution today, between 0-1524 m according to Wheeler (1992), it is usually found between 300-400 m depth (Mauchline, 1988). Combining the above results, the paleodepth is estimated less than 300 m for the basal sequence of Kalamaki section.

Considering the modern ecological data for the extant species present in the Kalamaki fish assemblage (Table 1), as well as the high occurrence of the extinct Mediterranean species *Diaphus cavallonis*, *D. rubus*, *D. cf. pedemontanus*, *Myctophum coppa*, and *Gadiculus labiatus*, which are typically recorded in the Miocene and Pliocene (Girone, 2007; Carnevale *et al.*, 2008; Girone *et al.*, 2010; Agiadi *et al.*, 2013a), the Kalamaki area was probably situated on the tropical-subtropical climatic zone border. Significant, in this respect, are the occurrences of tropical present-day extra-Mediterranean species *Physiculus* aff. *huloti* and *Diaphus taaningi*.

## 5.6 Magnetostratigraphy

The thermal demagnetization patterns and the trend of the magnetic susceptibility with increasing temperature clearly show two different behaviors in the pre-evaporitic unit and in the Trubi Formation of Kalamaki section (Fig. 2). The demagnetization patterns of both groups indicate that a low temperature component, probably of viscous origin, is sometimes demagnetized at 120°C. A second, normally-oriented component is demagnetized up to 210°-330° C and generally contributes with 70-80% to the initial magnetization in the pre-evaporitic interval and with 50%-70% in the Trubi Formation. This component is interpreted as an overprint of the present day field; in fact, in geographic coordinates, its mean declination is 0.7° N and the inclination is 54.5° (N=52; A95=2.7°), which are values very close to the present day

1  
2  
3  
4  
5  
6  
7  
8  
9  
10  
11  
12  
13  
14  
15  
16  
17  
18  
19  
20  
21  
22  
23  
24  
25  
26  
27  
28  
29  
30  
31  
32  
33  
34  
35  
36  
37  
38  
39  
40  
41  
42  
43  
44  
45  
46  
47  
48  
49  
50  
51  
52  
53  
54  
55  
56  
57  
58  
59  
60

field direction in the area of Zakynthos (3.79° N of declination and 54.05° of inclination). Samples collected in the pre-evaporitic sequence have a weak magnetization, showing a mean normal remanent magnetization (NRM) of 4.07 E-04 A/m (with a standard deviation of 6.02 E-04). Usually, an abrupt increase in magnetic susceptibility to 350°-420° C is detected, concomitant with an increase of the remanent magnetization, both indicative of authigenic sulphides. Besides the low-temperature components, a higher temperature component is rarely isolated in this group above 210°C. In several samples, the characteristic component (ChRM) is isolated between 230 and 350° C. This component exhibits both normal and reversed polarities (Fig. 12). Normal polarities are identified in the following intervals: a) from the base of the section to 0.6 m, the Zijderveld diagrams for this samples display a linear decay towards the origin; b) at 2.55 m; c) from 8.58 to 12.03 m. Sample with reversed polarities are identified at 6.53 m, at 14.02 m, and at 20.15 m. The Zijderveld diagrams of interval b) and c) and of reversed polarity samples all show a cluster of demagnetization steps. Mean direction for normal and reversal polarities were calculated by mean of Fisher's statistics and are 64.3°/39.8° (N=12, k=21.6° and  $\alpha_{95}=9.6^\circ$ ) and 230.1°/-50.0° (N=4, k=13.9° and  $\alpha_{95}=25.6^\circ$ ). The second group of samples, collected in the Trubi section, displays a higher mean NRM (2.25 E-03 A/m, with a standard deviation of 1.92 E-03). Here, the demagnetization patterns show much more stable trends with respect to the pre-evaporitic samples. The ChRM is successfully recognized in all the samples between 210-230°C and a maximum of 560°C. Both reversed (KAL 142 to KAL 154; 194.3°/ -64.7°, N=5, k=9.17 and  $\alpha_{95}=26.7^\circ$ ) and normal (KAL 156 to KAL 174; 39.5°/42.2°, N=15, k=38.8 and  $\alpha_{95}=6.2^\circ$ ) polarities are recognized and the reversal is identified between 9.6 and 10.4 m.

**5.7 Stable oxygen and carbon isotopes**

In the pre-evaporitic sequence of Kalamaki section, bulk sediment and planktonic foraminiferal  $\delta$  values vary widely ( $-2.71 < \delta^{18}\text{O}_{\text{carb}}\text{‰} < 7.45$ ;  $-4.32 < \delta^{13}\text{C}_{\text{carb}}\text{‰} < 1.94$ ;  $-1.44 < \delta^{18}\text{O}_{\text{foram}}\text{‰} < 3.73$ ;  $-2.90 < \delta^{13}\text{C}_{\text{foram}}\text{‰} < 0.95$ ), with heavier values measured in the massive and calcareous marls (Fig. 14). Oxygen- and carbon-isotope compositions are consistent with the major late Miocene-early Pliocene paleoclimatic and paleoceanographic phases in the eastern Mediterranean Sea (Blanc-Valleron *et al.*,

2002; Krijgsman *et al.*, 2002; Kouwnhoven *et al.*, 2006), yet they present certain differentiations attributed to local factors. The background  $\delta^{13}\text{C}_{\text{carb}}$  value is  $\sim 1.5\text{‰}$ ; up to 14 m from the section base, the values increase only once, at the upper part of the massive marls, reaching values up to  $2\text{‰}$ . From 15 m until the end of the pre-evaporitic sequence,  $\delta^{13}\text{C}$  values exhibit no particular trend. The  $\delta^{18}\text{O}_{\text{carb}}$  record displays some positive shifts, revealing a “pulse” of higher salinity/evaporation that is more intense near the evaporitic unit. Additionally, there is a simultaneous decrease in  $\delta^{13}\text{C}_{\text{carb}}$  values and an increase in  $\delta^{18}\text{O}_{\text{carb}}$  values at the same stratigraphic level.

Wacey *et al.* (2008) suggested that such a phenomenon may be the result of isotopically-light carbon influence from bacterial sulfate reduction, due to increased stagnation at the beginning of sulfate deposition. Similar trends in both carbon and oxygen isotopes were described in the Legnagnone section (Northern Apennines, Italy) by Gennari *et al.* (2013). There is a remarkable similarity between the  $\delta^{18}\text{O}_{\text{carb}}$  and the  $\delta^{18}\text{O}_{\text{foram}}$  isotope records of Kalamaki pre-evaporitic sequence, suggesting that  $\delta^{18}\text{O}_{\text{foram}}$  values reflect the variability of salinity, evaporation, and fresh water input. In the upper part of the PLG (cycle H),  $\delta^{13}\text{C}_{\text{carb}}$  values mostly fluctuate around  $-4\text{‰}$ , while  $\delta^{18}\text{O}_{\text{carb}}$  values range between  $-5$  and  $8\text{‰}$  (Fig. 15). The most prominent change, linked to environmental phenomena, seems to be the positive  $\delta^{18}\text{O}$  shift ( $\sim 8\text{‰}$ ) recorded just below and above the gypsum bed, revealing high salinity that is consistent with the evaporite deposition (cycles A-G). The observed negative  $\delta^{18}\text{O}_{\text{carb}}$  shifts of more than  $1\text{‰}$  are considered indicative of increased freshwater input. Sharp  $\delta^{13}\text{C}_{\text{carb}}$  negative and positive shifts characterize rapid changes in the hydraulic budget and in the ventilation of the basin, from lacustrine to saline conditions (Shackleton *et al.*, 1995).

The M/P boundary is marked by the first excursion toward higher  $\delta$  values ( $\delta^{18}\text{O}_{G. obliquus} = -0.75\text{‰}$ ,  $\delta^{13}\text{C}_{G. obliquus} = 0.91\text{‰}$ ) that occurs at the base of the Trubi Formation (Fig. 15). In contrast to the presence of abundant planktonic assemblages above the M/P boundary level, the freshwater influence remains significant over an interval corresponding to five cm of sediment marked by negative  $\delta^{18}\text{O}$  values (black shale just below the Trubi). This development reflects the rapid transition to marine conditions at the onset of the Pliocene. The establishment of stable normal marine conditions is recorded 20 cm above the M/P boundary. Above this level,  $\delta^{18}\text{O}_{G. obliquus}$  oscillations correspond to the ten (I to X) cycles of the Trubi Formation (Shackleton *et al.*, 1995; Di Stefano & Sturiale, 2010), with  $\delta^{18}\text{O}$  values varying at a range of

1  
2  
3  
4  
5  
6  
7  
8  
9  
10  
11  
12  
13  
14  
15  
16  
17  
18  
19  
20  
21  
22  
23  
24  
25  
26  
27  
28  
29  
30  
31  
32  
33  
34  
35  
36  
37  
38  
39  
40  
41  
42  
43  
44  
45  
46  
47  
48  
49  
50  
51  
52  
53  
54  
55  
56  
57  
58  
59  
60

approximately 1.5‰ in each cycle. The overlying early Pliocene sediments rapidly stabilize at positive  $\delta^{13}\text{C}$  values ( $0.32 < \delta^{13}\text{C}_{\text{‰}} < 1.39$ ), characteristic of an open-marine, stable, and well-ventilated environment. Moreover, the  $\delta^{13}\text{C}$  signal follows the same frequency changes as the  $\delta^{18}\text{O}$ , with the transitions to lighter  $\delta^{13}\text{C}$  values coinciding with high shifts to heavier  $\delta^{18}\text{O}$  values (Fig. 13). The simultaneous  $\delta^{18}\text{O}$  increase and  $\delta^{13}\text{C}$  decrease are possibly related to sea surface temperature variations and reveal that the glacial cycles (Sprovieri *et al.*, 2006) also influenced the eastern Mediterranean during the early Pliocene.

**5.8 Strontium isotopes**

The results of the strontium isotope analyses in the Kalamaki section gypsum unit are presented in Fig. 2. Selenite samples yield  $^{87}\text{Sr}/^{86}\text{Sr}$  values of 0.708993 for ( $2\sigma = 0.0014$ ) and 0.709007 ( $2\sigma = 0.0015$ ). These values correspond to PLG deposits from stage 1 of the salinity crisis (Roveri *et al.*, 2014a,b).

**6. Discussion**

**6.1 Chronostratigraphic framework**

The observed distributions of planktonic foraminifer and calcareous nannofossil species were used to recognize astronomically-tuned bioevents that are already defined in lower Messinian Mediterranean sections (Krijgsman *et al.*, 1999; Hilgen & Krijgsman, 1999; Sierro *et al.*, 2001; Blanc-Valleron *et al.*, 2002; Manzi *et al.*, 2011; Manzi *et al.*, 2013) (Figure 14). The first peak of *T. multiloba* is recognized one meter from the base of the western Kalamaki subsection and can be correlated with its first abundant occurrence dated at 6.415 Ma in the Perales section (Sierro *et al.*, 2001). The first abundant occurrence of dextral *N. acostaensis*, identified also in the Perales section and dated at 6.339 Ma, is recorded at 2.7 m. This biostratigraphic event is considered more reliable than the *N. acostaensis* coiling change as no sinistral specimens were observed below this level. The presence of *G. scitula* at 3.7 m can be correlated with its first influx and dated between 6.291-6.287 Ma. The interval between 8.8-9.2 m, dominated by sinistral *N. acostaensis*, is correlated with the relevant interval found in the Metochia section (Gavdos Island; Drinia *et al.*, 2007) and in the Perales composite section (Sierro *et al.*, 2001; Manzi *et al.*, 2013), and it is

dated between 6.140-6.108 Ma. The influx of *T. multiloba* at 9 m can be correlated with a relevant influx of this species at Perales section, which falls in the upper part of cycle UA28, dated at 6.121 Ma. The influx of *G. scitula* at 9.3 m correlates well with the second known influx of this species, dated between 6.105 and 6.099 Ma (Sierro *et al.*, 2001). The dominance of sinistral *N. acostaensis* identified at 10.4 m can be correlated with the second influx of sinistral *N. acostaensis* dated between 6.078 and 6.08 Ma, approximately at the same level of the influx of *T. multiloba* at 10.5 m, which could correspond to the last prominent influx of the species in the Perales section. The oligotypic assemblage recorded below the slumped interval and the high abundance of planktonic foraminifera at 14.3 m were also observed in the Sorbas basin and in the Northern Apennines (Sierro *et al.*, 2003; Gennari *et al.*, 2013) preceding the last eccentricity maximum centered at ca. 6.01 Ma, before the onset of the MSC.

Based on this biostratigraphic framework, the normal polarity at the lower part of the Kalamaki pre-evaporitic sequence (up to 0.68 m) is correlated with subchron C3An.2n (6.733-6.436 Ma after Lourens *et al.*, 2004), below the first abundant occurrence of *T. multiloba*. The reverse magnetic signal at 6.53 m falls within subchron C3An.1r. This interval is confirmed by the position of the *N. acostaensis* dextral-coiling specimens' abundant occurrence and the *G. scitula* first influx. The normal polarities between 8.58 and 12.03 m correlate with subchron C3An.1n (6.252-6.033 Ma) and the reversal polarities at 14.02-20.15 m fall within the lower part of subchron C3r.

As for the calcareous nannofossil, the typical specimens of *D. quinquerramus*, usually recorded in other pre-evaporitic deposits (e.g. Gavdos Island; Triantaphyllou *et al.*, 1999), is not found in the Kalamaki sequence, probably due to the establishment of a semi-closed, neritic, littoral environment (Wade *et al.*, 2006). However, the presence of *N. amplificus* supports the biostratigraphic assignment of the Kalamaki pre-evaporitic unit within the NN11 biozone, dated between 6.82-5.98 Ma (Raffi *et al.*, 2006; Backman *et al.*, 2012).

Reworked planktonic foraminifera and nannofossil specimens characterize the upper part of the PLG succession and the Lago Mare deposits in the Kalamaki section. *Gephyrocapsa* spp. specimens, although suggesting an age within the early Pliocene (subbottom of *Gephyrocapsa* spp. at 4.33 Ma; Lourens *et al.*, 2004), were also observed in the late Messinian pre-evaporitic diatomites of Gavdos (Triantaphyllou *et*



1  
2  
3  
4  
5  
6  
7  
8  
9  
10  
11  
12  
13  
14  
15  
16  
17  
18  
19  
20  
21  
22  
23  
24  
25  
26  
27  
28  
29  
30  
31  
32  
33  
34  
35  
36  
37  
38  
39  
40  
41  
42  
43  
44  
45  
46  
47  
48  
49  
50  
51  
52  
53  
54  
55  
56  
57  
58  
59  
60

*al.*, 1999). Thus, their presence in the Kalamaki sequence contributes to the limited knowledge on the precise stratigraphic and geographic distribution of these early representatives of the genus in the SE Mediterranean region.

Just before the Trubi Formation (Fig. 15), the planktonic foraminifera assemblages in both Kalamaki and Ag. Sostis sections are assigned to the Transitional Unit identified in the ODP sections by Iaccarino *et al.* (1999). In sample KAL 134, the rare presence of calcareous nannofossil *Ceratolithus acutus*, together with specimens of *Reticulofenestra zancleana*, implies an age within the base of the NN12 biozone, in the early Zanclean (5.36 Ma; Di Stefano & Sturiale, 2010; Backman *et al.*, 2012).

The M/P boundary (5.33 Ma) is defined by the distribution of dextral and sinistral forms of *N. acostaensis* and the *Sphaeroidinellopsis* Acme Base, further supported by the increasing of the oxygen and carbon isotope values, and it is placed at the base of the Trubi Formation. The recognized bioevents and the polarity reversal identified in the lower part of Trubi Formation of Kalamaki section are correlated with the upper part of subchron C3r and the normal polarity at the C3r/C3n boundary is placed in the 9.6-10.4 m interval midpoint (event IV; Fig. 15) dated at 5.235 Ma (Lourens *et al.*, 2004), below the *Sphaeroidinellopsis* Acme End (5.21 Ma). The sinistral shifts of *N. acostaensis* at 7.8 and 8.52 m are ascribed to the first and second *N. acostaensis* sinistral shifts that are reported from several Mediterranean Lower Pliocene sections (Di Stefano *et al.*, 1996; Lourens *et al.*, 1996; Iaccarino *et al.*, 1999; Pierre *et al.*, 2006; Gennari, 2007; Drinia *et al.*, 2008), dated at 5.330 and 5.281 Ma (Lourens *et al.*, 2004) and correlated with the base of cycle 2-top cycle 1 and the base of cycle 2-top cycle 3, respectively. The base of the *Sphaeroidinellopsis* Acme Zone, recorded at 8.3 m, and its top, at 11.3 m, correspond to the cycle 2 and the base of cycle 6, respectively. The first common occurrence of *Globorotalia margaritae* (FCO) is recorded in KAL 171 and marks cycle 10, dated at 5.08 Ma (Lourens *et al.*, 2004). Consequently, the studied Trubi Formation sediments belong to the MPL1 biozone – lower part of the MPL2 biozone; its base may be correlated with the base of the Zanclean, as defined in the Eraclea Minoa GSSP at 5.33 Ma (Van Couvering *et al.*, 2000). The presences of *Sphenolithus* spp. (abundance >5%), *Reticulofenestra pseudoumbilicus* (abundance 1-2%, possibly representing the *R. pseudoumbilicus* Pliocene Paracme Zone; Di Stefano & Sturiale, 2010), rare *Reticulofenestra zancleana*, and several discoasterid species (*D. brouweri*, *D. pentaradiatus*, *D. surculus*, *D. intercalaris*, *D. variabilis*); in conjunction with the common occurrence

of *Amaurolithus* spp.; document the biostratigraphic correlation with the nannofossil biozone NN12 (Martini, 1971), or MNN12a-b (Rio *et al.*, 1990). Therefore, the Trubi sediments of Kalamaki section (Fig. 15) have an early Zanclean age, ranging between 5.36-5.0 Ma.

## 6.2 Kalamaki paleoenvironmental reconstruction

The fish assemblage identified in the pre-evaporitic Messinian of Kalamaki section (Fig. 2) is indicative of a coastal marine area, with easy access to the open ocean, not exceeding 300 m in its deeper parts. The great diversity of the fauna, along with the fact that it incorporates deep-water pelagic species, such as *Maurolicus muelleri*, *Gadiculus argenteus* and *Physiculus* aff. *huloti*, as well as shallow-water inhabitants, such as gobiids, suggests that fossils from different adjacent underwater domains were combined during deposition. This light transport effect is commonly observed in the otolith faunas (Agiadi *et al.*, 2013b), and it is the result of a high bathymetric gradient in the area of deposition. Thus, the Kalamaki area paleogeographic scheme proposed here is further supported by this observation. Several paleoenvironmental changes can be recognized by the variations of the faunal and isotopic markers resulted to a step-wise progression towards the evaporitic conditions.

### 6.2.1 Pre-evaporitic sequence

#### Interval 6.45-6.121 Ma (0-9 m)

In the pre-evaporitic sequence of Kalamaki (KAL 10-50; Figure 2), the nannofossil assemblage of *H. carteri*, *C. leptoporus*, *U. jafari*, *R. haqii*, and *R. minutula* is mostly represented by whole coccospheres, indicating high productivity and fresh-water input to the surface waters (e.g., Triantaphyllou *et al.*, 2009). In addition, the impressive monospecific assemblages of *Sphenolithus abies* in the upper part of the pre-evaporitic sequence (samples KAL 45-55 and 85-92) suggest marine mesotrophic environments (Wade *et al.*, 2006).

In this basal part of the pre-evaporitic sequence, the bulk sediment  $\delta^{18}\text{O}$  values range between 0-2.1‰, reflecting marine conditions with slight salinity and/or temperature fluctuations (Fig. 13). The positive trend of  $\delta^{13}\text{C}$  reveals high productivity related to cold waters. The oligotypic planktonic foraminifera record is characterized by levels with 60-100% dominance of *T. multiloba*. This species is related to progressive isolation of the Mediterranean, and it is thought to be tolerant to increased salinity

1  
2  
3  
4  
5  
6  
7  
8  
9  
10  
11  
12  
13  
14  
15  
16  
17  
18  
19  
20  
21  
22  
23  
24  
25  
26  
27  
28  
29  
30  
31  
32  
33  
34  
35  
36  
37  
38  
39  
40  
41  
42  
43  
44  
45  
46  
47  
48  
49  
50  
51  
52  
53  
54  
55  
56  
57  
58  
59  
60

(Sierro et al., 2001). Its occurrence together with *T. quinqueloba* and *G. glutinata* in this part of the section is related to cold and nutrient rich surface waters (Tolderlund and Bé, 1971; Sierro *et al.*, 2003). The almost complete absence of planktonic foraminifera 2-4 m from the base is associated with increased riverine input causing a reduction of the sea surface salinity. This is further supported by the  $\delta^{18}\text{O}$  negative excursions and nannofossil assemblages indicative of high productivity and fresh-waters input. At around 3.7 m, normal marine conditions are inferred by the oxygen isotope positive values around 1‰ accompanied by the *G. scitula* influx, which is a deep-dwelling species (Bè and Tolderlund, 1971). The return to positive  $\delta^{18}\text{O}$  values suggest that the negative values recorded below this level are due to a temporary restriction of the Atlantic connection, during a sea level-fall, or excess precipitation in the Mediterranean area at this time. Maximum  $\delta^{18}\text{O}$  values, corresponding to hypersalinity episodes, alternate with values near 0‰ (between 7-9 m), which reflect periods when normal marine conditions prevailed. In these high-salinity levels, the planktonic foraminiferal assemblage is dominated by *G. glutinata* and *T. quinqueloba*; the sporadic presence of *T. multiloba* is also noted. High abundance of these species usually occurs under conditions of environmental stress and is also related to decreased food availability and low water-temperatures, reflecting the climatic variability toward a cooling phase around 6.121 Ma (Van der Laan *et al.*, 2005; Gennari *et al.*, 2013). It is hypothesized that stressful conditions for the marine meiofauna were induced by an increase of surface-water salinity. The foraminiferal isotopic composition ( $\delta^{18}\text{O}$  and  $\delta^{13}\text{C}$ ) is related to the ecological affinities of the species involved. *Turborotalita multiloba* is considered a morphotype of *T. quinqueloba* with more chambers in the final whole. The former species proliferates near river-influenced, low temperature, and nutrient-rich waters, and it tolerates increased salinities (Bè and Tolderlund, 1971). Hence, its isotopic composition directly reflects salinity and/or temperature variations. The parallel low  $\delta^{13}\text{C}$  values with high  $\delta^{18}\text{O}$  values may be related to an average increase of salinity in the lower part of sequence.

Interval 6.122-5.97 Ma (9-22 m)

The nannoflora assemblages are indicative of marine mesotrophic environments in the upper part of the basal Kalamaki sequence. Toward the top and before the deposition of the gypsum,  $\delta^{18}\text{O}$  varies between -4 and 8‰, suggesting that salinity fluctuates

rapidly between highly evaporated and diluted conditions (Bellanca *et al.*, 2001). Foraminiferal carbon and oxygen isotopes of this interval were analyzed on *Orbulina universa*. Since this species proliferates in mixed-layer surface waters during surface water stratification, the isotopic compositions reflect changes in temperature, fresh water input, or trophic content (Sierro *et al.*, 2003). There is a 4‰ difference between the  $\delta^{13}\text{C}$  values in the upper and lower part of the basal Kalamaki interval. This probably reflects the contrast between nutrient-depleted waters of the stratified summer mixed layer, recorded in the upper part of the basal sequence, and the increased nutrient availability of the basal interval ( $\delta^{13}\text{C}$  in *T. multiloba*). A cooling phase punctuated by hypersaline conditions is centered at 12 m, and may be delimited by the levels of increased fresh-water input and the warmer phases evidenced by the fish fauna and planktonic foraminifera assemblages. Indeed, the fish fauna is dominated by warm-water species, notably *Diaphus taaningi* and *Physiculus* aff. *huloti* in the intervals below and over this cooling phase, whereas these taxa are completely absent in the cooling phase, which is characterized by the presence of *Maurolicus muelleri* mostly preferring temperate conditions. The onset of MSC is accompanied by the disappearance of plankton assemblages, heavier oxygen isotopic values and a sharp negative carbon isotope shift.

#### Post-evaporitic sequence

The establishment of rather eutrophic conditions may be hypothesized, based on the presence of small placoliths, along with the siliciclastic nature of the sediments at the uppermost part of the Kalamaki Lago-Mare unit, just before the onset of Trubi Formation (e.g., Young, 1994). The samples from approximately one meter below the Agios Sostis Trubi Formation (Fig. 7) contain (AS 20-23) moderately preserved nannofossil assemblages and more reworked material with respect to the Kalamaki samples, indicating greater land proximity.

In the interval 5.6-5.33 Ma (1.4-7.5 m), from the top of the gypsum unit to the beginning of the Trubi Formation, the bulk sediment  $\delta^{18}\text{O}$  values vary widely from 8‰ in the gypsum to -6‰ in the upper part of the sequence. The calcite  $\delta^{13}\text{C}$  values fluctuate between -6 and -1‰ (Fig. 13). These isotopic values reflect wide variations of the paleoenvironmental conditions from hypersaline conditions to fresh and brackish water.

1  
2  
3  
4  
5  
6  
7  
8  
9  
10  
11  
12  
13  
14  
15  
16  
17  
18  
19  
20  
21  
22  
23  
24  
25  
26  
27  
28  
29  
30  
31  
32  
33  
34  
35  
36  
37  
38  
39  
40  
41  
42  
43  
44  
45  
46  
47  
48  
49  
50  
51  
52  
53  
54  
55  
56  
57  
58  
59  
60

The total nannofossil content in the interval just above the Miocene/Pliocene (M/P) boundary in the Kalamaki section implies warm surface-water conditions in a pelagic environment. In particular, the presence of discoasterids, *Rhabdosphaera* spp., *Sphenolithus* spp., *Scyphosphaera* spp., *Amaurolithus* spp. is indicative of warm subtropical conditions (e.g., Rio & Sprovieri, 1986). Relatively increased productivity is inferred by the presence of *Helicosphaera carteri*, a species preferring warm waters and moderately-elevated nutrient-levels. The faunal assemblages as well as the isotope analyses reveal stable paleoenvironmental conditions settled at the beginning of the Zanclean, due to the restoration of normal marine conditions.

**6.3 Zakynthos Neogene paleogeographic and structural evolution**

Field observations suggest that the Neogene sediments in the main part of Zakynthos Island were deposited over the Pre-Apulian zone formations, whereas those in the southeastern part were deposited over the Ionian zone. The correlation of the field observations with the available borehole data and the onshore seismic section (Figs. 1, 9, and 10) reveals that the Neogene formations over the Pre-Apulian zone sediments, east of the Vrahionas anticline (Fig. 1), form a monocline dipping approximately 30° ESE. Borehole stratigraphy (Fig. 9) indicates that the Neogene deposits (gypsum included) increase their thickness toward the dipping monocline.

The Neogene sediments exhibit their maximum thickness (800-1350 m) within the largest depocenter zone, extending eastward from the Agios Sostis area. The westernmost gypsum outcrops (Ploumari) consist of eradicated PLG blocks, whereas the easternmost ones (Panagia) contain gypsum turbidites and gypsum cumulates (Fig. 1). Consequently, the PLG deposits accumulated in a shallow marine basin (Fig. 13), which was located in the western part of the Zakynthos (Alikanas) basin (west of the Ploumari outcrops; Fig. 1), and they were almost completely eroded during late Messinian. Indeed, about one km north of the Keri village (Fig. 1), in the Perlakia location, early Pliocene conglomerates and sandstones lie over the early-middle Miocene marls through an angular unconformity. Thus, the eroded PLG deposits provided the clastic material that was deposited as gypsum turbidites (RLG) along the Messinian basin slope (Panagia outcrops) and in its depocenter.

On the contrary, Neogene sediments over the Ionian zone formations in the south-easternmost part of the island are considerably thinner (200-300 m). Gypsum deposits in Kalamaki and Argassi areas correspond to MSC stage 1 PLG unit; to the east

(Skopos area, Fig. 1), only some rare and small gypsum outcrops can be observed, mainly reworked gypsum and occasionally gypsum turbidites. These differences suggest that the Zakynthos Neogene basin was not uniform, but subsidence in the monocline area (over Pre-Apulian basement) was more rapid as compared with the eastern area (over Ionian basement).

The above observations are explained by a simple model of continental foreland-directed migration of the Hellenide (Alpine) thrusting, during the late Neogene and Pliocene. The Ionian thrust foreland basin can be modeled according to the foreland basin systems proposed by DeCelles & Giles (1996), although it is necessary to take into consideration the particular role of the Ionian Triassic evaporites diapiric movements (Karakitsios, 1995). The Neogene formations over the Pre-Apulian zone correspond to the foredeep, the forebulge and flank between them; those overlying Ionian zone rocks correspond to the wedge-top (Fig. 14). The greater subsidence characterizing the foredeep and flank-to-forebulge areas is reflected in the increased thickness of the clastic Neogene formations over the Pre-Apulian zone (between 800-1350 m), which partially derived from the eroded Pre-Apulian forebulge.

Simultaneously, the diapiric movement of the Ionian Triassic evaporites prevented substantial subsidence to occur. As a result, the eastern part of the Neogene basin over the Ionian zone basement corresponds to a slowly-subsiding wedge-top. This is reflected in the observed thin clastic Neogene sediments derived from the Ionian orogen's erosion.

During the Messinian, the shallow depths in the wedge-top and forebulge area of the basin, together with the upper Messinian overall negative hydrological balance (Mertz-Kraus *et al.*, 2009) led to the deposition of the PLG. The subsequent PLG erosion produced clastic gypsum that was deposited through gravity-flows in the slope and the depocenter. In addition, PLG mass-flows were accumulated in the distal Zakynthos foreland slope. By the end of the Messinian, the PLG unit was completely eroded at the forebulge zone, probably due to subaerial exposure. The MES (Fig. 14) is located directly above the pre-evaporitic sequence west of the Ploumari gypsum outcrops (Fig. 1), and it passes over the remaining PLG in the proximal slope (Ploumari gypsum outcrops). In the distal slope and the foreland depocenter, the MES becomes a correlative conformity.

The wedge-top zone was characterized by shallower depths, mainly due to the diapiric uplift of the Ionian Triassic evaporites (Karakitsios, 1995). Indeed, the sea depth in

1  
2  
3  
4  
5  
6  
7  
8  
9  
10  
11  
12  
13  
14  
15  
16  
17  
18  
19  
20  
21  
22  
23  
24  
25  
26  
27  
28  
29  
30  
31  
32  
33  
34  
35  
36  
37  
38  
39  
40  
41  
42  
43  
44  
45  
46  
47  
48  
49  
50  
51  
52  
53  
54  
55  
56  
57  
58  
59  
60

the Kalamaki area, prior to the PLG deposition, is estimated around 300 m, based on the fish assemblages. Consequently, the Kalamaki area, placed over the external Ionian Triassic diapir (Agia Dynati diapir; Figs. 1 and 14), received PLG deposits. Eroded gypsum material from the wedge-top PLG also supplied clastic gypsum to the foredeep RLG unit, which was located to its west (Fig. 14).

In the Argassi area, PLG was also deposited over the Agios Ioannis diapir; the upper PLG part was subsequently eroded. Quaternary erosion obscures the continuation of the deposited sediments of this area. Possibly the Argassi and Kalamaki sections during PLG deposition belonged to the same evaporitic basin that was separated by an early activation of the Agios Ioannis diapir (Fig. 14 A).

The proposed paleogeographic scheme for the last period of the Trubi Formation's deposition is presented in Fig. 14 B. The Lago-Mare unit lies unconformably over the MES in the wedge-top (Kalamaki area), whereas in the distal slope and in the depocenter it was deposited with a correlative conformity. The Trubi Formation succeeds the Lago-Mare unit, in stratigraphic continuity. The onset of the Trubi Formation at 5.33 Ma, corresponding to the Pliocene flooding of the Mediterranean basin, is recorded well on Zakynthos Island.

The present results indicate that the Messinian gypsum units of Zakynthos Island were deposited in a Mediterranean peripheral/marginal sub-basin context (*sensu* Roveri *et al.*, 2014a), formed during the late Messinian in the Pre-Apulian foreland basin, before the early Pliocene main deformation phase responsible for the tectonic emplacement of the Ionian zone over the Pre-Apulian zone.

**7. Conclusions**

The present detailed study identifies the Messinian evaporitic basins on Zakynthos Island, whose dynamics were controlled by the inherent substratum properties and the regional tectonic regime. The development and distribution of the depositional environments, before the Ionian thrust activation, was mainly influenced by the Triassic evaporites diapiric movements in the foreland basin. The Zakynthos Messinian evaporites were deposited in Mediterranean peripheral/marginal sub-basins. The PLG was accumulated in the shallower parts (<300 m) of the Zakynthos foreland basin, formed over the Pre-Apulian and the Ionian Alpine basement. In the areas over Pre-Apulian basement, the Neogene sequence consists of mass-wasting Messinian gypsum, which passes to mainly gypsum turbidites indicating a deeper

environment. These deposits derived from the dismantlement and resedimentation of the PLG unit and correspond to the RLG.

Planktonic foraminifera and calcareous nannoplankton biostratigraphy, magnetostratigraphic analysis, and correlation with astronomically-tuned Mediterranean sections provide the chronostratigraphic framework for the studied sequences. The pre-evaporitic sequence in Kalamaki section is dated between 6.415-6.01 Ma. Nine planktonic foraminiferal bioevents are distinguished. In Kalamaki section, PLG was deposited during the first MSC stage, between 5.971-5.60 Ma. The resedimented PLG deposits observed in Agios Sostis area correspond to the second MSC stage (5.6-5.55 Ma). The M/P boundary is placed at the base of the Trubi Formation, dated at 5.33 Ma. The Kalamaki section Trubi Formation, corresponds to the interval between 5.33-5.08 Ma, in which five planktonic foraminiferal bioevents were distinguished.

Two intervals are distinguished through the paleoenvironmental reconstruction of the pre-evaporitic Messinian in Kalamaki area: a) 6.45-6.122 Ma and b) 6.122-5.97 Ma. During the first interval (6.45-6.122 Ma), marine conditions prevailed, with slight salinity and temperature variations. The positive  $\delta^{13}\text{C}$  trend and the oligotypic planktonic foraminiferal assemblage, dominated by *T. multiloba*, indicate high-productivity cold waters. Between approximately 6.2-6.14 Ma (7-9 m), high  $\delta^{18}\text{O}$  corresponding to hypersalinity episodes alternate with normal salinity conditions with decreased food availability and low temperature. Between 6.122-5.97 Ma, marine mesotrophic conditions are well established; the isotopic record suggests nutrient-depleted waters of the stratified summer mixed layer. Both the planktonic foraminifera and the fish assemblage indicate a cooling phase punctuated by hypersalinity episodes around 6.05 Ma (12 m). In the upper part of the pre-evaporitic sequence, the observed synchronous decrease in the carbon isotopic ratio, and increase in the oxygen isotopic ratio may be caused by isotopically-light carbon input from bacterial sulfate reduction, due to increasing stagnation conditions at the beginning of sulfate deposition. After the MSC, eutrophic conditions are indicated at the uppermost part of the Lago-Mare facies unit, just before the onset of Trubi limestone Formation.

A new paleogeographic and structural model, integrating all the observed data, is proposed. In the Zakynthos foreland basin, the Neogene formations over Ionian zone correspond to the wedge-top, consistently with the diapiric movements of the Ionian



1  
2  
3  
4  
5  
6  
7  
8  
9  
10  
11  
12  
13  
14  
15  
16  
17  
18  
19  
20  
21  
22  
23  
24  
25  
26  
27  
28  
29  
30  
31  
32  
33  
34  
35  
36  
37  
38  
39  
40  
41  
42  
43  
44  
45  
46  
47  
48  
49  
50  
51  
52  
53  
54  
55  
56  
57  
58  
59  
60

Triassic evaporites, whereas those overlying the Pre-Apulian zone correspond to the foredeep and the flank, between foredeep and forebulge. PLG erosion, both at the forebulge and the wedge-top, supplied the foreland basin’s depocenter with gypsum turbidites. The PLG unit at the forebulge zone was totally eroded and the MES is now located directly above the pre-evaporitic sequence, while, it is over the remaining PLG in the slope area, and it became a correlative conformity for subsequent sediments at the depocenter zone of the foreland basin. In the wedge-top zone, the MES over the upper part of PLG unit is overlapped by the Lago-Mare unit, over which the Trubi Formation lies in stratigraphic continuity.

**Acknowledgments**

This research has been co-financed by the European Union (European Social Fund – ESF) and Greek national funds through the Operational Program "Education and Lifelong Learning" of the National Strategic Reference Framework (NSRF) - Research Funding Program: THALIS-UOA-“Messinian Salinity Crisis: the greatest Mediterranean environmental perturbation and its repercussions to the biota”.

***No conflict of interest declared***

**References**

AGIADI, K. (2013) *Investigation of the Plio-Pleistocene eastern Mediterranean Ichthyofauna and paleoenvironmental representations on Rhodes and Crete Islands*, PhD Thesis, University of Athens.

AGIADI, K., TRIANTAPHYLLOU, M., GIRONE, A., KARAKITSIOS, V. & DERMITZAKIS, M. (2010) Paleobathymetric interpretation of the fish otoliths from the lower - middle quaternary deposits of Kephallonia and Zakynthos islands (Ionian Sea, Western Greece). *Rivista Italiana di Paleontologia e Stratigrafia*, 116(1), 63-78.

AGIADI, K., KOSKERIDOU, E., TRIANTAPHYLLOU, M., GIRONE, A. & KARAKITSIOS, V. (2013) Fish otoliths from the Pliocene Heraklion Basin (Crete Island, Eastern Mediterranean). *Geobios*, 46, 461-472.

ANTONARAKOU, A., DRINIA, H., TSAPARAS, N. & DERMITZAKIS, M.D., (2007). Micropaleontological Micropaleontological parameters as proxies of late

1  
2  
3 Miocene surface water properties and paleoclimate in Gavdos Island, eastern  
4 Mediterranean. *Geodiversitas*, 29(3), 379-399.

5  
6  
7 AUBRY, M.-P. (1984, 1988, 1989, 1990, 1999) *Handbook of Cenozoic Calcareous*  
8 *Nannoplankton*. Vol. 1-5, Micropress, American Museum of Natural History, New  
9 York.  
10

11  
12  
13 BACKMAN, J., RAFFI, I., RIO, D., FORNACIARI, E. & PÄLIKE, H. (2012)  
14 Biozonation and biochronology of Miocene through Pleistocene calcareous  
15 nannofossils from low and middle latitudes. *Newsletters on Stratigraphy*, 45(3), 221-  
16 244.  
17  
18

19  
20  
21 BAUMANN, K.-H., ANDRULEIT, H., BÖCKEL, B., GEISEN, M. & KINKEL, H.  
22 (2005) The significance of extant coccolithophores as indicators of ocean water  
23 masses, surface water temperature, and paleoproductivity: a review. *Paläontologische*  
24 *Zeitschrift*, 79, 93-112.  
25  
26

27  
28 BÈ, A.W.H., TOLDERLUND, D.S. (1971) *Distribution and ecology of living*  
29 *planktonic foraminifera in surface waters of the Atlantic and Indian Oceans*. In:  
30 Funnel, B.M., Riedel, W.R. (Eds.), *The Micropaleontology of Oceans*. Cambridge  
31 University Press, Cambridge, pp. 105-149.  
32  
33

34  
35  
36 BELLANCA, A., CARUSO, A., FERRUZZA, G., NERI, R., ROUCHY, J.M.,  
37 SPROVIERI, M. & BLANC-VALLERON, M.M. (2001) Transition from marine to  
38 hypersaline conditions in the Messinian Tripoli Formation from the marginal areas of  
39 the central Sicilian Basin. *Sedimentary Geology*, 140(1-2), 87-105.  
40  
41

42  
43  
44 BIRCK, J. (1986) Precision K–Rb–Sr isotope analysis: application to Rb–Sr  
45 chronology. *Chemical Geology*, 56, 73-83.  
46  
47

48  
49 BLANC-VALLERON, M.-M., PIERRE, C., CAULET, J.P., CARUSO, A.,  
50 ROUCHY, J.-M., CESPUGLIO, G., SPROVIERI, R., PESTREA, S. & DI  
51 STEFANO, E. (2002) Sedimentary, stable isotope and micropaleontological records  
52 of paleoceanographic change in the Messinian Tripoli Formation (Sicily, Italy).  
53 *Palaeogeogr. Palaeoclimatol. Palaeoecol.*, 185, 255-286.  
54  
55  
56  
57  
58  
59  
60

- BOWN, P.R., & YOUNG, J.R. (1998) Techniques. In: *Calcareous Nannofossil Biostratigraphy* (Ed. by P.R. Bown), pp. 16–28, Kulwer Academic Publications, Dordrecht.
- BP CO. LTD. (1971.) *The Geological results of petroleum exploration in western Greece. Institute for Geology and Subsurface Research (now I.G.M.E.).* Special Report, 10, Athens.
- BUTLER, R.W.H., LICKORISH, W.H., GRASSO, M., PEDLEY, H.M. & RAMBERTI, L. (1995) Tectonics and sequence stratigraphy in Messinian basins, Sicily: constraints on the initiation and termination of the Mediterranean salinity crisis. *Geolog. Soc. America Bull.*, 107(4), 425-439.
- CARNEVALE, G., LANDINI, W. & SARTI, G. (2006) Mare versus Lago-mare: marine fishes and the Mediterranean environment at the end of the Messinian Salinity Crisis. *Journal of the Geological Society London*, 163, 75-80.
- CARNEVALE, G., LONGINELLI, A., CAPUTO, D., BARBIERI, M. & LANDINI, W. (2008) Did the Mediterranean marine reflooding precede the Mio–Pliocene boundary? Paleontological and geochemical evidence from upper Messinian sequences of Tuscany, Italy. *Palaeogeography, Palaeoclimatology, Palaeoecology*, 257(1-2), 81-105.
- CHADIMA, M., & HROUDA, F. (2006) Remas of t 3.0 a User friendly Paleomagnetic Data Browser and Analyzer. *Travaux Géophysiques*, 27, 20-21.
- CIESM (2008) The Messinian salinity crisis from mega-deposits to microbiology. A consensus report. In: *33ème CIESM Workshop Monographs* (Edited by F. Briand), pp. 91-96, Monaco.
- COHEN, D.M., INADA, T., IWAMOTO, T. & SCIALABBA, N. (1990) FAO species catalogue. Vol.10. Gadiform fishes of the world (Order Gadiformes). An annotated and illustrated catalogue of cods, hakes, grenadiers and other gadiform fishes known to date. *FAO Fish. Synop.*, 125(1), pp. 442, FAO, Rome.
- CROS, L. (2001) *Planktonic coccolithophores of the NW Mediterranean*, PhD thesis, pp.181, Departament d'Ecologia, Universitat de Barcelona, Barcelona.

- DERMITZAKIS M. (1977) Stratigraphy and sedimentary history of the Miocene of Zakynthos (Ionian Islands, Greece). *Ann. Geol. Pays Hell.*, 29, 47-186.
- DECELLES, P.G. & GILES, K.A. (1996) Foreland basin systems. *Basin Research*, 8(2), 105-123.
- DE LANGE, G.J., & KRIJGSMAN, W. (2010) Messinian Salinity Crisis: a novel unifying shallow gypsum/ deep dolomite formation mechanism. *Marine Geology*, 275, 273-277.
- DELA PIERRE, F., CLARI, P., BERNARDI, E., NATALICCHIO, M., COSTA, E., CAVAGNA, S., LOZARA, F., LUGLI, S., MANZI, V., ROVERI, M. & VIOLANTI, D. (2012) Messinian carbonate-rich beds of the Tertiary Piedmont Basin (NW Italy): Microbially-mediated products straddling the onset of the salinity crisis. *Palaeogeography, Palaeoclimatology, Palaeoecology*, 344-345, 78-93.
- DIMIZA, M.D., TRIANTAPHYLLOU, M.V., DERMITZAKIS, M.D. (2008) Seasonality and ecology of living coccolithophores in E. Mediterranean coastal environments (Andros Island, Middle Aegean Sea). *Micropaleontology*, 54, 159-175.
- DIMIZA, M.D., TRIANTAPHYLLOU, M.V. & MALINVERNO, E. (2014) New evidence for the ecology of *Helicosphaera carteri* in polluted coastal environments (Elefsis Bay, Saronikos Gulf, Greece). *Journal of Nannoplankton Research*, 34, special issue Coccolithophores 2014 INA workshop.
- DI STEFANO, A. & STURIALE, G. (2010) Refinements of calcareous nannofossil biostratigraphy at the Miocene/Pliocene Boundary in the Mediterranean region. *Geobios*, 43, 5-20.
- DI STEFANO, E., SPROVIERI, R. & SCARANTINO, S. (1996) Chronology of biostratigraphic events at the base of the Pliocene. *Paleopelagos*, 6, 401-414.
- DRINIA, H., ANTONARAKOU, A., TSAPARAS, N. & KONTAKIOTIS, G. (2007) Palaeoenvironmental conditions preceding the MSC: a case study from Gavdos Island. *Geobios*, 40, 251-265.

1  
2  
3  
4  
5  
6  
7  
8  
9  
10  
11  
12  
13  
14  
15  
16  
17  
18  
19  
20  
21  
22  
23  
24  
25  
26  
27  
28  
29  
30  
31  
32  
33  
34  
35  
36  
37  
38  
39  
40  
41  
42  
43  
44  
45  
46  
47  
48  
49  
50  
51  
52  
53  
54  
55  
56  
57  
58  
59  
60

DRINIA, H., ANTONARAKOU, A., KONTAKIOTIS, G., (2008). On the occurrence of Early Pliocene marine deposits in the Ierapetra Basin, Eastern Crete, Greece. *Bulletin of Geosciences*, 83(1), 63-78.

DUERMEIJER, C.E., KRIJGSMAN, W., LANGEREIS, C.G., MEULENKAMP, J.E., TRIANTAPHYLLOU, M.V. & ZACHARIASSE, W.J. (1999) A late Pleistocene clockwise rotation phase of Zakynthos (Greece) and implications for the evolution of the western Aegean arc. *Earth and Planetary Science Letters*, 173(3), 315-331.

FABRICIUS, F.H., HEIMANN, K.O. & BRAUNE, K. (1998) Comparison of site 274 with circum-Ionian land sections: implications for the Messinian “salinity crisis” on the basis of a dynamic model. *Initial reports DSDP*, 42, 927-942.

FLECKER, R., DE VILLIERS, S. & ELLAM, R.M. (2002) Modelling the effect of evaporation on the salinity–87Sr/86Sr relationship in modern and ancient marginal-marine systems: the Mediterranean Messinian Salinity Crisis. *Earth and Planetary Science Letters*, 203(1), 221-233.

FLORES, J.A., SIERRO, F.J., FILIPPELLI, G.M., BÁRCENA, M.A., PÉREZ-FOLGADO, M., VÁZQUEZ, A. & UTRILLA, R. (2005) Surface water dynamics and phytoplankton communities during deposition of cyclic late Messinian sapropel sequences in the western Mediterranean. *Mar. Micropaleontol.*, 56, 50-79.

FROESE, R. & PAULY, D. (2014) *FishBase*. World Wide Web electronic publication, [www.fishbase.org](http://www.fishbase.org), version (08/2014).

FORTUIN, A.R. & KRIJGSMAN, W. (2003) The Messinian of the Nijar Basin (SE Spain): sedimentation, depositional environments and paleogeographic evolution. *Sedimentary Geology*, 160(1-3), 213-242.

GARCIA-CASTELLANOS, D., ESTRADA, F., JIMÉNEZ-MUNT, I., GORINI, C., FERNÁNDEZ, M., VERGÉS, J. & DE VICENTE, R. (2009) Catastrophic flood of the Mediterranean after the Messinian salinity crisis. *Nature*, 462, 778-781.

GENNARI, R. (2007) *Cause e modalità della formazione messiniana “LagoMare” e passaggio al Pliocene*, Ph. D. Thesis, University of Parma, Parma, 126 pp.

1  
2  
3 GENNARI, R., IACCARINO S.M., DI STEFANO, A., STURIALE, G.,  
4 CIPOLLARI, P., MANZI, V., ROVERI, M. & COSENTINO, D. (2008) The  
5 Messinian – Zanclean boundary in the Northern Apennine. *Stratigraphy*, 5(3-4), 307-  
6 322.  
7  
8

9  
10 GENNARI, R., MANZI, V., ANGELETTI, L., BERTINI, A., BIFFI, U.,  
11 CEREGATO, A., FARANDA, C. GLIOZZI, E. LUGLI, S., MENICHETTI, E.,  
12 ROSSO, A. ROVERI, M. & TAVIANI, M. (2013) A shallow water record of the  
13 onset of the Messinian salinity crisis in the Adriatic foredeep (Legnagnone section,  
14 Northern Apennines). *Palaeogeography, Palaeoclimatology, Palaeoecology*, 386,  
15 145-164.  
16  
17

18  
19 GIRONE, A., NOLF, D. & CAVALLO, O. (2010) Fish otoliths from the pre-  
20 evaporitic (Early Messinian) sediments of northern Italy: their stratigraphic and  
21 palaeobiogeographic significance. *Facies*, 56, 399-432.  
22  
23

24  
25 GIGNOUX, M. (1936) *Géologie stratigraphique*. 2nd édition, pp. 709, Masson, Paris.  
26  
27

28  
29 HEMLEBEN, CH., SPINDLER, M., ANDERSON, O.R. (1989) *Modern Planktonic*  
30 *Foraminifera*. Springer, New York, pp. 1-363.  
31  
32

33  
34 HILGEN, F.L. & KRIJGSMAN, W. (1999) Cyclostratigraphy and astrochronology of  
35 the Tripoli diatomite formation (pre-evaporite Messinian, Sicily, Italy). *Terra Nova*,  
36 11, 16-22.  
37  
38

39  
40 HILGEN, F., KUIPER, K., KRIJGSMAN, W., SNEL, E. & VAN DER LAAN, E.,  
41 (2007) Astronomical tuning as the basis for high resolution chronostratigraphy: the  
42 intricate history of the Messinian Salinity Crisis. *Stratigraphy*, 4(2/3), 231-238.  
43  
44

45  
46 HSU, K.J., RYAN, W.B.F. & CITA, M.B. (1973) Late Miocene desiccation of the  
47 Mediterranean. *Nature*, 242, 240-244.  
48  
49

50  
51 IACCARINO, S.M., PREMOLI SILVA, I., BIOLZI, M., FORESI, L.M., LIRER, F.,  
52 TURCO, E., & PETRIZZO, M.R. (2007) *Practical manual of Neogene planktonic*  
53 *foraminifera*, 1-180. Perugia: Università di Perugia Press International School on  
54 Planktonic Foraminifera, (Neogene Planktonic Foraminifera).  
55  
56  
57  
58  
59  
60

1  
2  
3  
4  
5  
6  
7  
8  
9  
10  
11  
12  
13  
14  
15  
16  
17  
18  
19  
20  
21  
22  
23  
24  
25  
26  
27  
28  
29  
30  
31  
32  
33  
34  
35  
36  
37  
38  
39  
40  
41  
42  
43  
44  
45  
46  
47  
48  
49  
50  
51  
52  
53  
54  
55  
56  
57  
58  
59  
60

IACCARINO, S.M., BERTINI, A., DI STEFANO, A., FERRARO, L., GENNARI, R., GROSSI, F., LIRER, F., MANZI, V., MENICHETTI, E., RICCI LUCCHI, M., TAVIANI, M., STURIALE, G. & ANGELETTI, L. (2008) The Trave section (Monte dei Corvi, Ancona, Central Italy): an integrated paleontological study of the Messinian deposits. *Stratigraphy*, 5, 283-308.

IACCARINO, S., CASTRADORI, D., CITA, M.B., DI STEFANO, E., GABOARDI, S., MCKENZIE, J.A., SPEZZAFERRI, S. & SPROVIERI, R. (1999) The Miocene–Pliocene boundary and the significance of the earliest Pliocene flooding in the Mediterranean. *Mem. Soc. Geol. Ital.*, 54, 109-131.

IADANZA, A., SAMPALMIERI, G., CIPOLLARI, P., MOLA, M. & COSENTINO, D. (2013) The “Brecciated Limestones” of Maiella, Italy: Rheological implications of hydrocarbon-charged fluid migration in the Messinian Mediterranean Basin. *Palaeogeography, Palaeoclimatology, Palaeoecology*, 390, 130-147.

KARAKITSIOS, V. (1995). The influence of preexisting structure and halokinesis on organic matter preservation and thrust system evolution in the Ionian basin, northwestern Greece. *AAPG Bulletin*, 79, 960-980.

KARAKITSIOS, V. (2013) Western Greece and Ionian Sea petroleum systems. *AAPG Bulletin*, 97(9), 1567-1595.

KARAKITSIOS, V. & RIGAKIS, N. (2007) Evolution and petroleum potential of western Greece. *Journal of Petroleum Geology*, 30(3), 197-218.

KONTOPOULOS, N., ZELILIDIS, A., PIPER, D.J.W. & MUDIE, P.J. (1997) Messinian evaporites in Zakynthos, Greece. *Palaeogeography, Palaeoclimatology, Palaeoecology*, 129(3-4), 361-367.

KOUWENHOVEN, T.J. & VAN DER ZWAAN, G.J. (2006) A reconstruction of late Miocene Mediterranean circulation patterns using benthic Foraminifera. *Palaeogeography, Palaeoclimatology, Palaeoecology*, 238(1-4), 373-385.

KOUWENHOVEN, T.J., SEIDENKRANTZ, M.-S. & VAN DER ZWAAN, G.J. (1999) Deep-water changes: The near-synchronous disappearance of a group of

benthic Foraminifera from the late Miocene Mediterranean. *Palaeogeography, Palaeoclimatology, Palaeoecology*, 152, 259-281.

KOUWENHOVEN, T.J., HILGER, F.J. & VAN DER ZWAAN, G.J. (2003) Late Tortonian–early Messinian stepwise disruption of the Mediterranean–Atlantic connections: constraints from benthic foraminiferal and geochemical data. *Palaeogeography, Palaeoclimatology, Palaeoecology*, 198(3-4), 303-319.

KOUWENHOVEN, T.J., MORIGI, C., NEGRI, A., GIUNTA, S., KRIJGSMAN, W. & ROUCHY, J.-M. (2006) Paleoenvironmental evolution of the eastern Mediterranean during the Messinian: Constraints from integrated microfossil data of the Pissouri Basin (Cyprus). *Marine Micropaleontology*, 60(1), 17-44.

KRIJGSMAN, W., LANGEREIS, C.G., ZACHARIASSE, W.J., BOCCALETTI, M., MORATTI, G., GELATI, R., IACCARINO, S., PAPANI, G. & VILLA, G., (1999) Late Neogene evolution of the Taza-Guercif Basin (Riffian Corridor, Morocco) and implications for the Messinian salinity crisis. *Mar. Geol.*, 153(1-4), 147-160.

KRIJGSMAN, W., HILGEN, F.J., RAFFI, I., SIERRO, F.J. & WILSON, D.S. (1999b) Chronology, causes and progression of the Messinian salinity crisis. *Nature*, 400, 652-655.

KRIJGSMAN, W., BLANC-VALLERON, M.-M., FLECKER, R., HILGEN, F.J., KOUWENHOVEN, T.J., MERLE, D., ORSZEG-SPERBER, F. & ROUCHY, J.-M. (2002) The onset of the Messinian salinity crisis in the Eastern Mediterranean (Pissouri Basin, Cyprus). *Earth and Planetary Science Letters*, 194(3-4), 299-310.

LUGLI, S., SCHREIBER, B.C. & TRIBERTI, B. (1999) Giant Polygons in the Realmonte Mine (Agrigento, Sicily): Evidence for the Desiccation of a Messinian Halite Basin. *Journal of Sedimentary Research, Section A: Sedimentary Petrology and Processes*, 69(3), 764-771.

LUGLI, S., MANZI, V., ROVERI, M. & SCHREIBER, B.C. (2010) The Primary Lower Gypsum in the Mediterranean: A new facies interpretation for the first stage of the Messinian salinity crisis. *Palaeogeography Palaeoclimatology Palaeoecology*, 297, 83-99.



1  
2  
3  
4  
5  
6  
7  
8  
9  
10  
11  
12  
13  
14  
15  
16  
17  
18  
19  
20  
21  
22  
23  
24  
25  
26  
27  
28  
29  
30  
31  
32  
33  
34  
35  
36  
37  
38  
39  
40  
41  
42  
43  
44  
45  
46  
47  
48  
49  
50  
51  
52  
53  
54  
55  
56  
57  
58  
59  
60

LUGLI, S., GENNARI, R., GVIRTZMAN, Z., MANZI, V. & ROVERI, M., SCHREIBER, B.C. (2013) Evidence of Clastic Evaporites In the Canyons of the Levant Basin (Israel): Implications For the Messinian Salinity Crisis. *Journal of Sedimentary Research*, 83(11), 942-954.

LOURENS, L.J., ANTONARAKOU, A., HILGEN, F.J., VAN HOOFF, A.A.M., VERGNAUD-GRAZZINI, C. & ZACHARIASSE, W.J. (1996) Evaluation of the Plio-Pleistocene astronomical timescale. *Paleoceanography*, 11, 391-413.

LOURENS, L., HILGEN, F., SHACKLETON, N. J., LASKAR, J., & WILSON, J. (2004) The Neogene period. In: *A Geologic Time Scale 2004* (Edited by F. M. Gradstein *et al.*), p. 409-440, Cambridge University Press, Cambridge.

MALINVERNO, E., TRIANTAPHYLLOU, M.V., STAVRAKAKIS, S., ZIVERI, P. & LYKOUSIS, V. (2009) Seasonal and spatial variability of coccolithophore export production at the South-Western margin of Crete (Eastern Mediterranean). *Marine Micropaleontology*, 71, 131-147.

MANZI, V., LUGLI, S., RICCI LUCCHI, F. & ROVERI, M. (2005) Deep-water clastic evaporites deposition in the Messinian Adriatic foredeep (northern Apennines, Italy): did the Mediterranean ever dry out? *Sedimentology*, 52(4), 875-902.

MANZI, V., ROVERI, M., GENNARI, R., BERTINI, A., BIFFI, U., GIUNTA, S., IACCARINO, S.M., LANCI, L., LUGLI, S., NEGRI, A., RIVA, A., ROSSI, M.E. & TAVIANI, M. (2007) The deep-water counterpart of the Messinian Lower Evaporites in the Apennine foredeep: The Fanantello section (Northern Apennines, Italy). *Palaeogeography, Palaeoclimatology, Palaeoecology*, 251(3-4), 470-499.

MANZI, V., LUGLI, S., ROVERI, M. & SCHREIBER, B.C. (2009) A new facies model for the Upper Gupsum of Sicily (Italy): chronological and paleoenvironmental constraints for the Messinian salinity crisis in the Mediterranean. *Sedimentology*, 56: 1937-1960.

MANZI, V., LUGLI, S., ROVERI, M., SCHREIBER, B.C. & GENNARI, R. (2011) The Messinian “Calcare di Base” (Sicily, Italy) revisited. *Geological Society of America Bulletin*, 123(1-2), 347-370.

MANZI, V., GENNARI, R., LUGLI, S., ROVERI, M., SCAFETTA, N. & SCHREIBER, B.C. (2012) High-Frequency cyclicity in the Mediterranean Messinian evaporites: evidence for solar-lunar climate forcing. *Journal of Sedimentary Research*, 82(12), 991-1005.

MANZI, V., GENNARI, R., HILGEN, F., KRIJGSMAN, W., LUGLI, S., ROVERI, M. & SIERRO, F.J. (2013) Age refinement of the Messinian salinity crisis onset in the Mediterranean. *Terra Nova*, 25(4), 315-322.

MANZI, V., LUGLI, S., ROVERI, M., DELA PIERRE, F., GENNARI, R. LOZAR, F., NATALICCHIO, M., SCHREIBER, B.C., TAVIANI, M. & TURCO, E. (2015) The Messinian salinity crisis in Cyprus: a further step toward a new stratigraphic framework for Eastern Mediterranean. *Basin Research*, DOI: 10.1111/bre.12107.

MARTINI, E. (1971) Standard tertiary and quaternary calcareous nannoplankton zonation. In: *Proceedings of the 2nd Planktonic Conference* (Edited by A. Farinacci), p. 739-777, Edizioni Tecnioscienza, Rome.

MAUCHILNE, J. (1988) Growth and breeding of meso- and bathypelagic organisms of the Rockall Trough, northeastern Atlantic Ocean and evidence of seasonality. *Marine Biology*, 98, 387-393.

MEIJER, P.TH. & KRIJGSMAN, W. (2005) A quantitative analysis of the desiccation and re-filling of the Mediterranean during the Messinian Salinity Crisis. *Earth and Planetary Science Letters*, 240(2), 510-520.

MERTZ-KRAUS, R., BRACHERT, T.C., REUTER, M., GALER, S.J.G., FASSOULAS, C. & ILIOPOULOS, G. (2009) Late Miocene sea surface salinity variability and paleoclimate conditions in the Eastern Mediterranean inferred from coral aragonite  $\delta^{18}\text{O}$ . *Chemical Geology*, 262(3-4), 202-216.

MEZGER, E. (2012) *How dry was the Messinian salinity crisis? A molecular biogeochemical study of the Eraclea Minoa (Sicily) section, Italy*, pp.34, M.Sc. Thesis, Utrecht University, Utrecht.

NELSON, J.S. (2006) *Fishes of the World*, 4<sup>th</sup> ed., pp. 600, John Wiley and Sons Inc., New Jersey.

1  
2  
3  
4  
5  
6  
7  
8  
9  
10  
11  
12  
13  
14  
15  
16  
17  
18  
19  
20  
21  
22  
23  
24  
25  
26  
27  
28  
29  
30  
31  
32  
33  
34  
35  
36  
37  
38  
39  
40  
41  
42  
43  
44  
45  
46  
47  
48  
49  
50  
51  
52  
53  
54  
55  
56  
57  
58  
59  
60

NIKOLAOU, C. (1986) *Contribution to the knowledge of the Neogene, the geology and the Ionian and pre-Apulian limits in relation to the petroleum geology observations in Strophades, Zakynthos and Kephallinia islands*, pp. 228, PhD thesis, University of Athens, Athens.

NOLF, D. (1985) Otolithi Piscium, In: *Handbook of Paleoichthyology* (Edited by H.P. Schultze), vol. 10, pp. 145, Stuttgart.

NOLF, D. & BRZOBOHATY, R. (1994) Fish otoliths as paleobathymetric indicators. *Paleontologia i evolucion*, 24-25, 255-264.

OBIS (2006) *OBIS-extracted Depth Data*, Harvested by E.Agbayani July 2006 at [www.iobis.org](http://www.iobis.org).

OMODEO-SALE, S., GENNARI, R., LUGLI, S., MANZI, V. & ROVERI, M. (2012) Tectonic and climatic control on the Late Messinian sedimentary evolution of the Nijar Basin (Betic Cordillera, Southern Spain). *Basin Research*, 24(3), 314-337.

ORSZAG-SPERBER, F. (2006) Changing perspectives in the concept of “Lago-Mare” in Mediterranean Late Miocene evolution. *Sedimentary Geology*, 188-189, 259-277.

PAPANIKOLAOU, M., TRIANTAPHYLLOU, M., PLATZMAN, E., GIBBARD, P., MACNIOCAILL, C. & HEAD, M.J. (2011) A well-established Early–Middle Pleistocene marine sequence on SE Zakynthos island, Western Greece: magneto-biostratigraphic constraints and palaeoclimatic implications. *Journal of Quaternary Science*, 26, 523-540.

PERCH NIELSEN, K. (1985) Cenozoic calcareous nannofossils. In: *Plankton Stratigraphy* (Edited by Bolli, H.M., Saunders, J.B. & Perch-Nielsen, K.), p. 427-554, Cambridge Earth Science Series, Cambridge.

PIERRE, C., CARUSO, A., BLANC-VALLERON, M.-M., ROUCHY, J.M. & ORZSAG-SPERBER, F. (2006) Reconstruction of the paleoenvironmental changes around the Miocene-Pliocene boundary along a West-East transect across the Mediterranean, *Sedimentary Geology*, 188-189, 319-340.

1  
2  
3 RADE, J. (1975) Scyphosphaera evolutionary trends with special reference to eastern  
4 Australia. *Micropaleontology*, 21, 151-164.

6  
7 RAFFI, I., BACKMAN, J., FORNACIARI, E., PÄLIKE, H., RIO, D., LOURENS, L.  
8 & HILGEN, F. (2006) A review of calcareous nannofossil astrobiochronology  
9 encompassing the past 25 million years. *Quaternary Science Reviews*, 25, 3113-3137.

11  
12  
13 RICCI LUCCHI, F. (1973) *Sedimentologia*. Parte I. Materiali e tessiture dei  
14 sedimenti. Cooperativa libraria universitaria. Bologna.

16  
17  
18 RIO, D. & SPROVIERI, R. (1986) Biostratigrafia integrate del Pliocene-Pleistocene  
19 inferire Mediterraneo in un'ottica di stratigrafia systematica. *Boll. Soc. Paleontol.*  
20 *Italiana*, 25, 65-85.

22  
23  
24 ROBERTSON, A.H.F., EATON, S., FOLLOWS, E.J., PAYNE, A.S. (1995)  
25 Depositional processes and basin analysis of Messinian evaporites in Cyprus. *Terra*  
26 *Nova*, 7, 233-253.

28  
29  
30 ROUCHY, J.M. (1982) La genèse des évaporites messiniennes de Méditerranée.  
31 *Mém. Mus. Nat. Hist. Nat.*, C, 50, Paris.

32  
33  
34 ROUCHY, J.M. & CARUSO, A. (2006) The Messinian salinity crisis in the  
35 Mediterranean basin: a reassessment of the data and an integrated scenario.  
36 *Sedimentary Geology*, 188, 35-67.

38  
39  
40 ROVERI, M. & MANZI, V. (2006) The Messinian salinity crisis: looking for a new  
41 paradigm? *Palaeogeography, Palaeoclimatology, Palaeoecology*, 238, 386-398.

43  
44  
45 ROVERI, M., MANZI, V., BASSETTI, M.A., MERINI, M. & RICCI LUCCHI, F.  
46 (1998) Stratigraphy of the Messinian post-evaporitic stage in eastern-Romagna  
47 (northern Apennines, Italy). *Giornale di Geologia*, 60, 119-142.

49  
50  
51 ROVERI, M., MANZI, V., RICCI LUCCHI, F. & ROGLEDI, S. (2003) Sedimentary  
52 and tectonic evolution of the Vena del Gesso Basin (Northern Apennines, Italy):  
53 implications for the onset of the Messinian salinity crisis. *Geological Society of*  
54 *America Bulletin*, 115, 387-405.

1  
2  
3  
4  
5  
6  
7  
8  
9  
10  
11  
12  
13  
14  
15  
16  
17  
18  
19  
20  
21  
22  
23  
24  
25  
26  
27  
28  
29  
30  
31  
32  
33  
34  
35  
36  
37  
38  
39  
40  
41  
42  
43  
44  
45  
46  
47  
48  
49  
50  
51  
52  
53  
54  
55  
56  
57  
58  
59  
60

ROVERI, M., LUGLI, S., MANZI, V. & SCHREIBER, B.C. (2008a) The Messinian Sicilian stratigraphy revisited: new insights for the Messinian salinity crisis. *Terra Nova*, 20(6), 483-488.

ROVERI, M., BERTINI, A., COSENTINO, D., DI STEFANO, A., GENNARI, R., GLIOZZI, E., GROSSI, F., IACCARINO, S.M., LUGLI, S., MANZI, V. & TAVIANI, M. (2008b) A high-resolution stratigraphic framework for the latest Messinian events in the Mediterranean area. *Stratigraphy*, 5(3-4), 323-342.

ROVERI, M., FLECKER, R., KRIJGSMAN, W., LOFI, J., LUGLI, S., MANZI, V., SIERRO, F.J., BERTINI, A., CAMERLENGHI, A., DE LANGE, G., GOVERS, R., HILGEN, F.J., HÜBSCHER, C., MEIJER, P.T. & STOICA, M. (2014a) The Messinian Salinity Crisis: Past and Future of a great challenge for marine sciences. *Marine Geology*, 352, 25-58.

ROVERI, M., MANZI, V., BERGAMASCO, A., FALCIERI, F.M., GENNARI, R., LUGLI, S., SCHREIBER, B.C. (2014b) Dense shelf water cascading and Messinian canyons: a new scenario for the Mediterranean salinity crisis. *American Journal Of Science*, 314, 751-784.

ROVERI M., LUGLI S., MANZI V., GENNARI R. & SCHREIBER B.C. (2014c) High-resolution strontium isotope stratigraphy of the Messinian deep Mediterranean basins: implications for marginal to central basins correlation. *Marine Geology*, 349, 113-125.

RUGGIERI, G. (1967) The Miocene and later evolution of the Mediterranean Sea. In: *Aspects of Tethyan Biogeography, Systematics Association* (Edited by Adams, C.G. & Ager, A.V.), p. 283-290, London.

SHACKLETON, N.J., HALL, M.A. & PATE, D. (1995) Pliocene stable isotope stratigraphy of Site 846. *ODP Proc.*, 138, 337-355.

SELLI, R. (1954) Il Bacino del Metauro. *Giornale di Geologia*, 24, 1-294.

SIERRO, F.J., FLORES, J.A., ZAMARREÑO, I., VAZQUEZ, A., UTRILLA, R., FRANCES, G., HILGEN, F.J. & KRIJGSMAN, W. (1999) Messinian pre-evaporite

sapropels and precession-induced oscillations in western Mediterranean climate.

*Marine Geology*, 153, 137-146.

SIERRO, F.J., HILGEN, F.J., KRIJGSMAN, W. & FLORES, J.A. (2001) The Abad composite (SE Spain): A Mediterranean reference section for the Mediterranean and the APTS, *Palaeogeogr. Palaeoclimatol. Palaeoecol.*, 168, 141-169.

SIERRO, F.J., FLORES, J.A., FRANCÉS, G., VAZQUEZ, A., (2003) Orbitally controlled oscillations in planktic communities and cyclic changes in western Mediterranean hydrography during the Messinian. *Palaeogeography, Palaeoclimatology, Palaeoecology*, 190, 289-316.

SOREL, D. (1976) *Etude néotectonique dans l'arc égéen externe occidental*, pp. 200, Thèse 3<sup>e</sup> c., Paris XI, Paris.

SPROVIERI, R., SPROVIERI, M., CARUSO, A., PELOSI, N., BONOMO, S. & FERRARO, L. (2006) Astronomic forcing on the planktonic foraminifera assemblage in the Piacenzian Punta Piccola section (southern Italy). *Paleoceanography*, 21, PA4204.

TRANTAPHYLLOU, M.V. (1996) Biostratigraphical and ecostratigraphical observations based on calcareous nannofossils of the eastern Mediterranean Plio-Pleistocene deposits. *GAIA* 1, pp. 229.

TRANTAPHYLLOU, M.V., DRINIA, H. & DERMITZAKIS, M.D. (1997) The Plio-Pleistocene boundary in the Gerakas section, Zakynthos (Ionian Islands). *Neues Jahrbuch für Geologie und Paläontologie, Monatshefte*, 1, 12-30.

TRANTAPHYLLOU, M.V., TSAPARAS, N., STAMATAKIS, M. & DERMITZAKIS, M.D. (1999) Calcareous nannofossil biostratigraphy and petrological analysis of the preevaporitic diatomaceous sediments from Gavdos Island, southern Greece. *Neues Jahrbuch für Geologie und Paläontologie Monatshefte*, 3, 161-178.

TRANTAPHYLLOU, M.V., ZIVERI, P., GOGOU, A., MARINO, G., LYKOUSIS, V., BOULOUBASSI, I., EMEIS, K.-C., KOULI, K., DIMIZA, M., ROSELL-MELE, A., PAPANIKOLAOU, M., KATSOURAS, G. & NUNEZ, N. (2009a) Late Glacial-

1  
2  
3  
4  
5  
6  
7  
8  
9  
10  
11  
12  
13  
14  
15  
16  
17  
18  
19  
20  
21  
22  
23  
24  
25  
26  
27  
28  
29  
30  
31  
32  
33  
34  
35  
36  
37  
38  
39  
40  
41  
42  
43  
44  
45  
46  
47  
48  
49  
50  
51  
52  
53  
54  
55  
56  
57  
58  
59  
60

Holocene climate variability at the south-eastern margin of the Aegean Sea. *Marine Geology*, 266, 182-197.

TRIANAPHYLLOU, M.V., ANTONARAKOU, A., KOULI, K., DIMIZA, M., KONTAKIOTIS, G., PAPANIKOLAOU, M.D., ZIVERI, P., MORTYN, P.G., LIANOU, V., LYKOUSIS, V., DERMITZAKIS, M.D., (2009b). Late Glacial-Holocene ecostratigraphy of the south-eastern Aegean Sea, based on plankton and pollen assemblages. *Geo. Mar. Lett.*, 29(4), 249-267.

UNDERHILL, J.R. (1989) Late Cenozoic deformation of the Hellenide foreland, western Greece. *Geol. Society of America Bull.*, 101, 513-634.

YOUNG, J.R. (1994) Functions of coccoliths, In: *Coccolithophores* (Edited by Winter, A. & Siesser, W.G.), p. 63-82, Cambridge University Press, Cambridge.

VAI, G.B. (1997) Cyclostratigraphic estimate of the Messinian stage duration. In: *Miocene stratigraphy: an integrated approach, Developments in Paleontology and Stratigraphy* (Edited by Montanari, A. Odin, G.S. Coccioni, R.), 15, 463-476.

VAN ASSEN, E., KUIPER, K.F., BARHOUN, N., KRIJGSMAN, W. & SIERRO, F.J. (2006) Messinian astrochronology of the Melilla Basin: Stepwise restriction of the Mediterranean–Atlantic connection through Morocco. *Palaeogeography, Palaeoclimatology, Palaeoecology*, 238, 15-31.

WACEY, D., KILBURN, M.R., MCLOUGHLIN, N., PARNELL, J., STOAKES, C.A., GOVERNOR, C.R.M. & BRASIER, M. (2008) Use of NanoSIMS in the search for early life on Earth: ambient inclusion trails in a c. 3400 Ma sandstone. *Journal of the Geological Society London*, 165, 43-53.

WADE, B.S. & BOWN, P.R. (2006) Calcareous nannofossils in extreme environments: The Messinian Salinity Crisis, Polemi Basin, Cyprus. *Palaeogeography, Palaeoclimatology, Palaeoecology*, 233(3-4), 271-286.

WHEELER, A. (1992) A list of the common and scientific names of fishes of the British Isles. *Journal of Fish Biology*, 41(1),1-37.

ZELILIDIS, A., KONTOPOULOS, N., AVRAMIDIS, P. & PIPER, D.J.W. (1998)  
Tectonic and sedimentological evolution of the Pliocene-Quaternary basins of  
Zakynthos Island, Greece: Case study of the transition from compressional to  
extensional tectonics. *Basin Research*, 10(4), 393.

ZIVERI, P., BAUMANN, K.H., BÖCKEL, B., BOLLMANN, J. & YOUNG, J.  
(2004) Biogeography of selected coccolithophores in the Atlantic Ocean, from  
Holocene sediments. In: *Coccolithophores: From Molecular Processes to Global  
Impact* (Edited by Thierstein, H. & Young, J.), p. 403-428, Springer Verlag.

### Figure captions

Fig. 1. Geological map of Zakynthos Island. The regional location is indicated in the  
inset map. Boreholes: Z1 (Zakynthos-1); Z2 (Zakynthos-2), Z3 (Zakynthos-3); LA1  
(Laganas-1); KB101 (Keri-well), AK1 (Agios Kyrikos-1), KY1 (Kypseli-1).

Fig. 2. Kalamaki composite section with lithology, samples' location, macrofossils of  
the pre-evaporitic sequence, the evaporitic unit (the PLG facies description is referred  
in the key), the top of the evaporitic unit, and the post-evaporitic sequence, and two Sr  
isotope values from the base and the top of the gypsum unit). M/P: Miocene/Pliocene  
boundary, pre-MSC: pre-Messinian Salinity Crisis part of the section, MES:  
Messinian Erosional Surface, samples *KAL* 1 to *KAL* 173 with their position in the  
section.

Fig. 3. The Kalamaki section's facies detail. a. Pre-evaporitic sequence, PLG: Primary  
Lower Gypsum; b. Uppermost portion of the Primary Lower Gypsum unit topped by  
the Lago-Mare unit, and by the Trubi Formation: Lago-Mare stratification is  
overlapping (yellow arrow) the MES (Messinian Erosional Surface); c. Gypsum  
laminite; d. Swallow-tail gypsum selenites; e. Bottom view of a branching selenite  
cone; f. Branching selenite facies.

Fig. 4. Primary Lower Gypsum (PLG) unit. Letters A to H: correspond to the eight  
cycles of depositional gypsum types observed in the PLG unit. The last cycle H  
corresponds to top of the PLG unit showed in figure 3 b, is overlain by the Lago-Mare



1  
2  
3  
4  
5  
6  
7  
8  
9  
10  
11  
12  
13  
14  
15  
16  
17  
18  
19  
20  
21  
22  
23  
24  
25  
26  
27  
28  
29  
30  
31  
32  
33  
34  
35  
36  
37  
38  
39  
40  
41  
42  
43  
44  
45  
46  
47  
48  
49  
50  
51  
52  
53  
54  
55  
56  
57  
58  
59  
60

(LM) unit through a low-angle unconformity. Evaporite facies of the PLG unit: EF1: Shale, EF2: Limestone, EF3: Massive selenite, EF4: Banded selenite, EF5: Branching selenite (EF5<sub>L</sub>: Gypsum laminite), EF7: Gypsudite, EF8: Gypsarenite (see also key of Fig. 2).

Fig. 5. Kalamaki-Argassi Primary Lower Gypsum unit correlation.

Fig. 6. Trubi Formation facies. Based on lithology, nine cycles (I to IX) of marly limestones alternating with marls are observed.

Fig. 7. Agios Sostis composite section: lithology, samples location, and facies characteristics of the different stratigraphic levels.

Fig. 8. Sedimentary facies details of the PLG and RLG units. Argassi area: a. selenite, b. branching selenite. Agios Sostis area: c. pre-evaporitic sequence and MES boundary with the overlying RLG unit, d. gypsum turbidites, e: convolute lamination, f: alternations of primary cumulate gypsum (CU) and clastic gypsarenite (AR) and gypsudite (GR).

Fig. 9. Zakynthos (Alikanas) basin wells positioned in a west-to-east direction (the wells' locations are indicated in fig. 1). Correlation of the borehole logs shows that the Neogene deposits (gypsum included) increase their thickness eastward. Agios Kyrikos-1 well (AK-1) revealed indirect indices of halite accumulation in the Messinian gypsum stratigraphic level.

Fig. 10. Alikanas basin seismic profile (modified from the initial representation by Marinescu; in Nikolaou, 1986). The seismic profile shows a) the position of the Ionian thrust, b) the eastward increase in the thickness of the Neogene deposits. The seismic line's location is indicated in Fig. 1. PL-PT: Pliocene-Pleistocene, Pl: Pliocene, LPl: lower Pliocene, Mes-g: Messinian gypsum, M-UM: middle-upper Miocene, LM: lower Miocene, P-Aps: pre-Neogene sequence of the Pre-Apulian zone, P-Ions: pre-Neogene sequence of the Ionian zone (Triassic evaporites), ITF: Ionian thrust front, Ne: undifferentiated Neogene, SP: shot point, sec: time in seconds.

Fig. 11. Fish otoliths discovered in the pre-evaporitic sequence of Kalamaki section.

Fig. 12. A: plots of VGP latitude of the West and East Kalamaki subsections. B: plots of ChRM directions corrected for bed tilting, full and empty red and purple circles represent normal and reversed mean direction for Kalamaki West and east subsection, respectively. C: Zijderveld diagrams with demagnetization paths of selected samples from the Kalamaki west subsection.

Fig. 13. Pre-evaporitic sequence, Upper Evaporites, Lago-Mare, and Trubi Formation carbon and oxygen stable isotopes.

Fig. 14. Chrostratigraphic framework of Kalamaki section's pre-evaporitic sequence and correlation with Perales section (Sorbas basin) (modified after Sierro *et al.*, 2001; Manzi *et al.*, 2013) and Falconara section (Caltanissetta basin) (modified after Blanc-Valleron *et al.*, 2002; Hilgen & Krijgsman, 1999; Manzi *et al.*, 2011) via the astronomical Insolation summer curve of Laskar *et al.* 2004 and GPTS of Lourens *et al.*, 2004. Bio-magnetostratigraphic events are: 1) FAO *T. multiloba*; 2) FAO dextral *N. acostaensis*; 3) *G. scitula* influx; 4) *N. acostaensis* dominance sinistral; 5) *T. multiloba* influx; 6) *G. scitula* influx; 7) dominance *N. acostaensis* sinistral; 8) Last abundant influx *T. multiloba*; 9) HO planktonic Foraminifera; I) top C3An.1n; II) boundary C3An.2n/C3r

Fig. 15. Kalamaki section age model of the PLG top portion, Lago-Mare, and Trubi Formation, correlated with insolation curve (based on Laskar *et al.*, 2004).

Fig. 16. Paleogeographic reconstruction.

A. During the Messinian, the Zakynthos (Alikanas) foreland basin was formed in front of the Ionian thrust. The Neogene formations deposited over the Pre-Apulian domain corresponded to the *foredeep* and the *flank* between foredeep and *forebulge*, whereas those overlying the Ionian zone corresponded to the *wedge-top*, which was uplifted due to the diapiric movements of the Ionian Triassic evaporites. In the 1<sup>st</sup> MSC stage, PLG was deposited on both *forebulge* and *wedge-top*. In the 2<sup>nd</sup> MSC stage, PLG was totally or partially eroded (creating the Messinian Erosional Surface;

1  
2  
3  
4  
5  
6  
7  
8  
9  
10  
11  
12  
13  
14  
15  
16  
17  
18  
19  
20  
21  
22  
23  
24  
25  
26  
27  
28  
29  
30  
31  
32  
33  
34  
35  
36  
37  
38  
39  
40  
41  
42  
43  
44  
45  
46  
47  
48  
49  
50  
51  
52  
53  
54  
55  
56  
57  
58  
59  
60

MES) and redeposited with *correlative conformity* mainly as gypsum turbidites (RLG unit) in the depocenter of the foreland basin.

B. During the end of the Messinian, in Kalamaki-Argassi *wedge-top area* the Lago-Mare sediments were unconformably overlying the Primary Lower Gypsum above the MES, while in the depocenter of the foreland basin they were conformably deposited over the Resedimented Lower Gypsum. The Zanclean flood was recorded on both areas by the conformable deposition of the Trubi Formation.

*With red raffled and continuous line the unconformity and the correlative conformity of the MES, respectively.*

Table 1.

The identified Teleost fish taxa in the pre-evaporitic Messinian of Kalamaki section. Taxa in bold are not present in the modern Mediterranean. Taxa marked with an asterisk are presently extinct. Present-day ecological data and the corresponding references are presented for the extant taxa. Climatic zone distributions are abbreviated as follows: Tr. Tropical, ST. Subtropical, Te. Temperate, SP. Subpolar. The modern ecology of *Buglossidium* sp. refers to its only present-day representative, *B. luteum* (Risso, 1810).

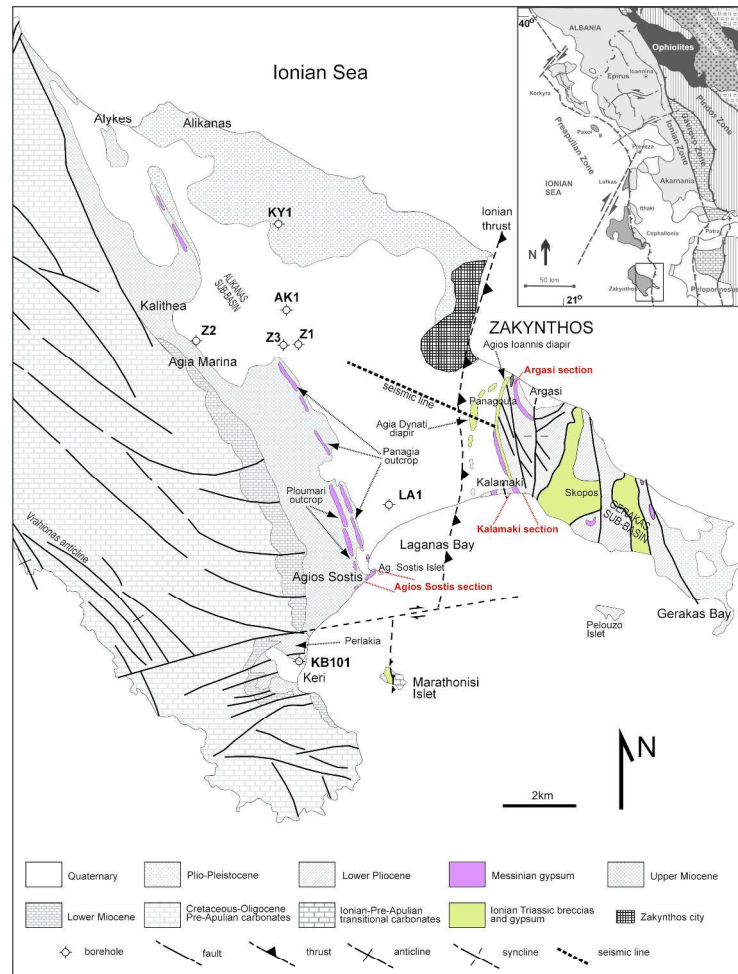


Fig. 1. Geological map of Zakynthos Island. The regional location is indicated in the inset map. Boreholes: Z1 (Zakynthos-1); Z2 (Zakynthos-2), Z3 (Zakynthos-3); LA1 (Laganas-1); KB101 (Keri-well), AK1 (Agios Kyrikos-1), KY1 (Kypseli-1). 209x297mm (300 x 300 DPI)

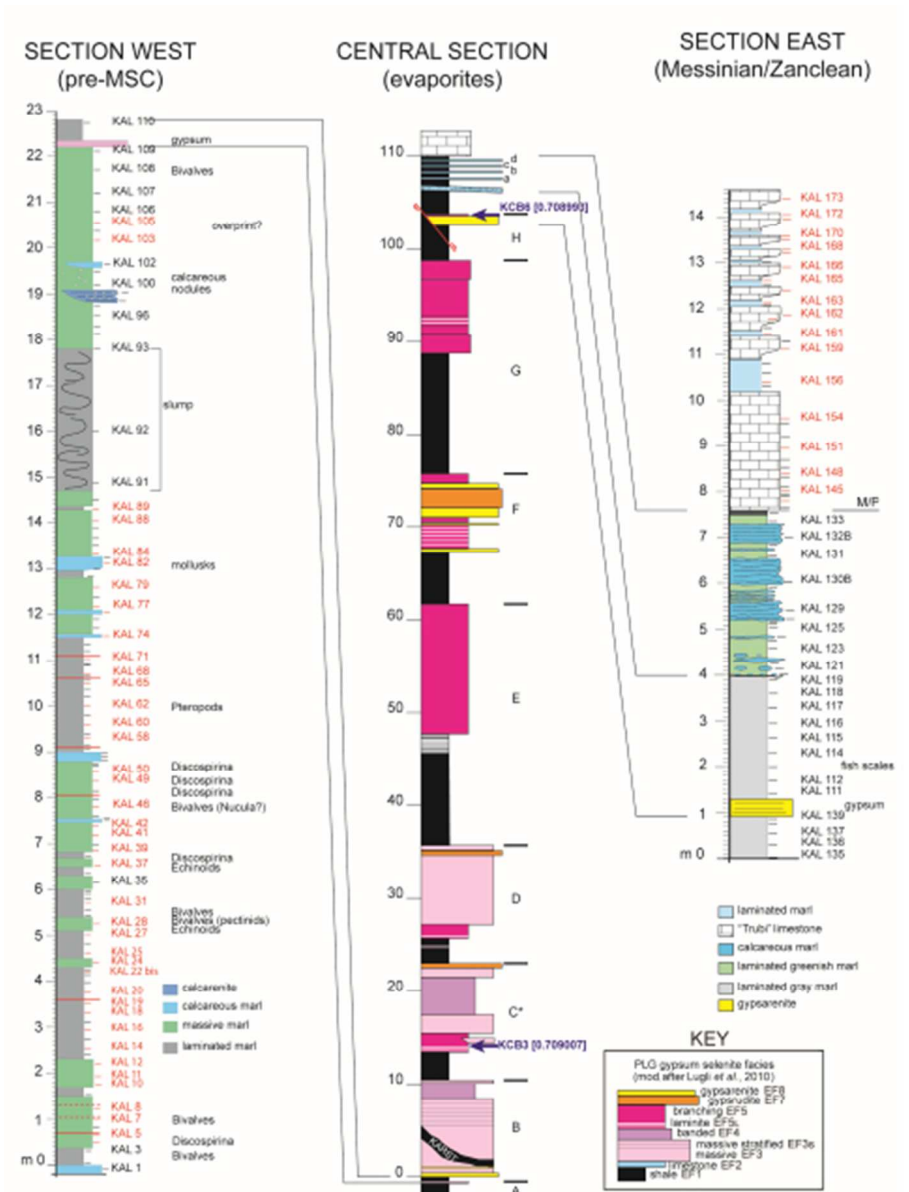


Fig. 2. Kalamaki composite section with lithology, samples' location, macrofossils of the pre-evaporitic sequence, the evaporitic unit (the PLG facies description is referred in the key), the top of the evaporitic unit, and the post-evaporitic sequence, and two Sr isotope values from the base and the top of the gypsum unit). M/P: Miocene/Pliocene boundary, pre-MSC: pre-Messinian Salinity Crisis part of the section, MES: Messinian Erosional Surface, samples KAL 1 to KAL 173 with their position in the section. 40x54mm (300 x 300 DPI)

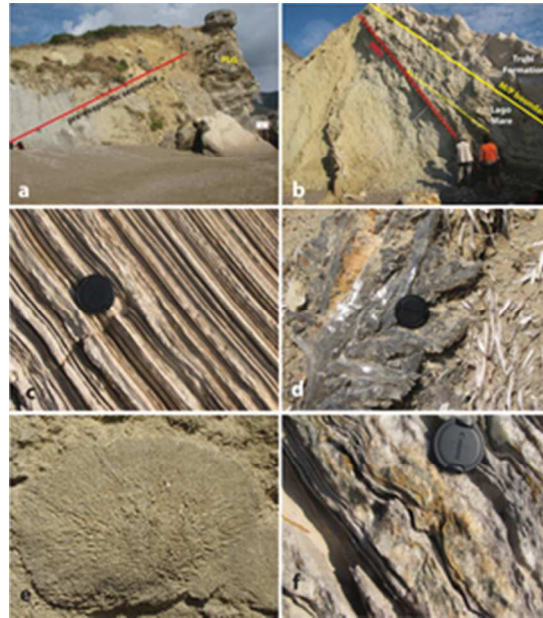


Fig. 3. The Kalamaki section's facies detail. a. Pre-evaporitic sequence, PLG: Primary Lower Gypsum; b. Uppermost portion of the Primary Lower Gypsum unit topped by the Lago-Mare unit, and by the Trubi Formation: Lago-Mare stratification is overlapping (yellow arrow) the MES (Messinian Erosional Surface); c. Gypsum laminite; d. Swallow-tail gypsum selenites; e. Bottom view of a branching selenite cone; f. Branching selenite facies.  
22x25mm (300 x 300 DPI)

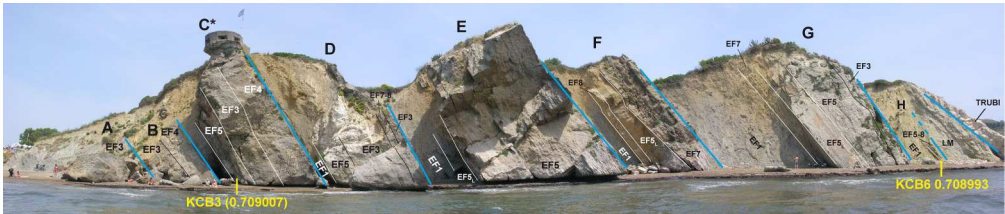


Fig. 4. Primary Lower Gypsum (PLG) unit. Letters A to H: correspond to the eight cycles of depositional gypsum types observed in the PLG unit. The last cycle H corresponds to top of the PLG unit showed in figure 3 b, is overlain by the Lago-Mare (LM) unit through a low-angle unconformity. Evaporite facies of the PLG unit: EF1: Shale, EF2: Limestone, EF3: Massive selenite, EF4: Banded selenite, EF5: Branching selenite (EF5L: Gypsum laminite), EF7: Gypsudite, EF8: Gypsarenite (see also key of Fig. 2).  
793x167mm (72 x 72 DPI)



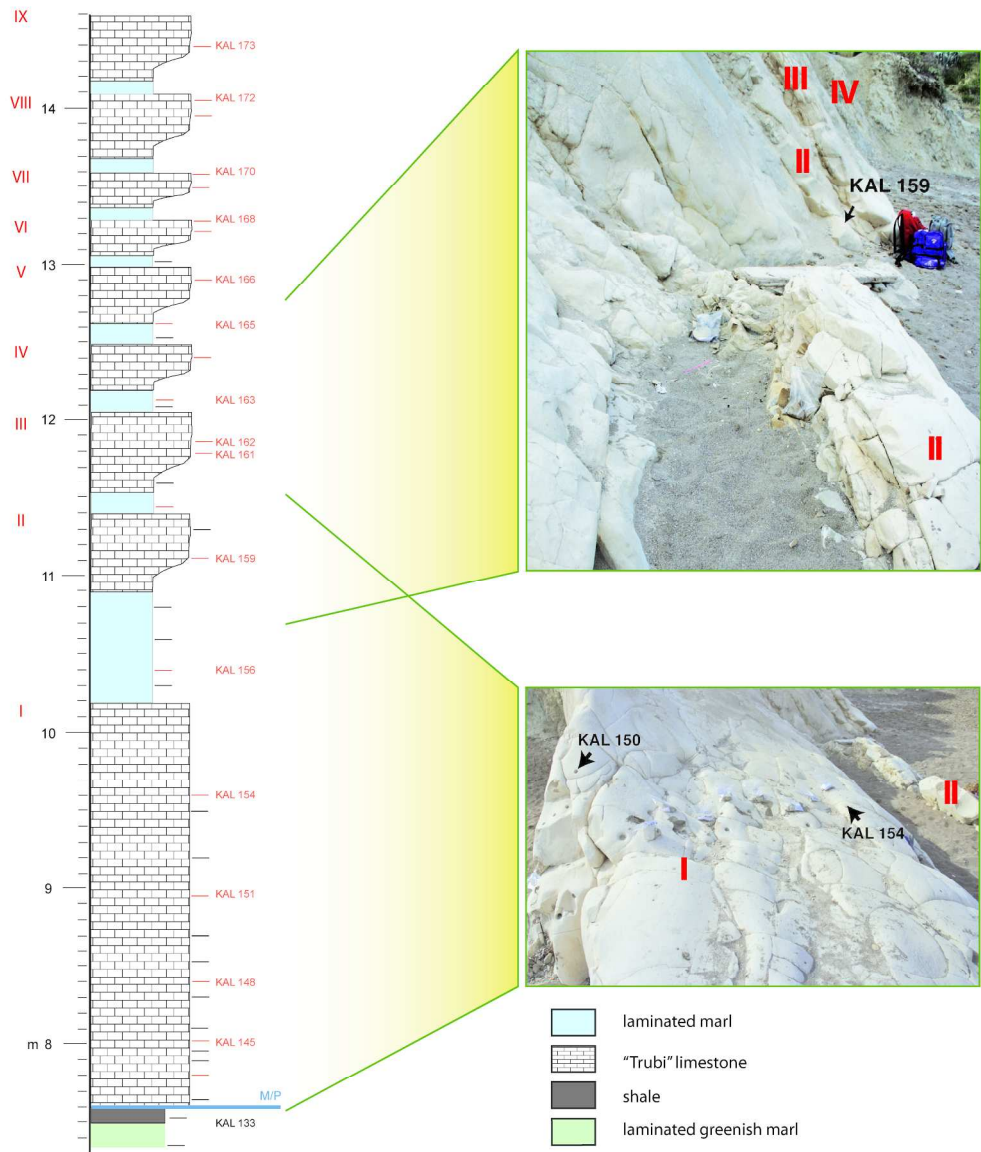


Fig. 5. Kalamaki-Argassi Primary Lower Gypsum unit correlation.  
203x241mm (300 x 300 DPI)



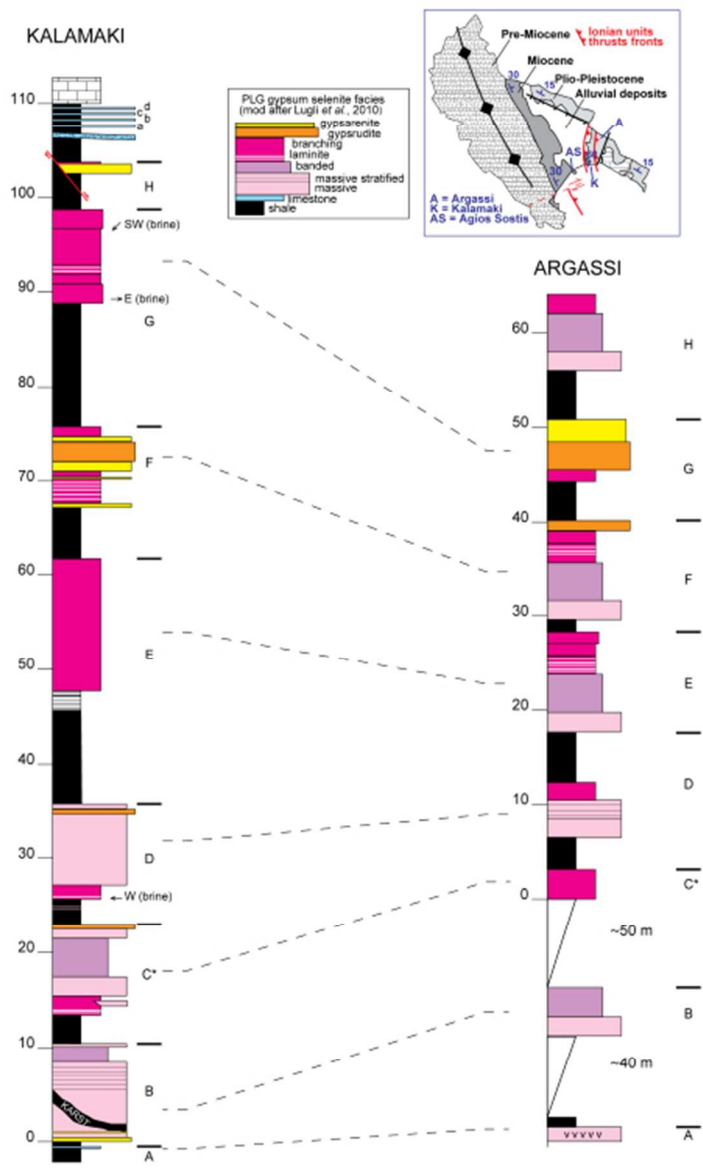


Fig. 6. Trubi Formation facies. Based on lithology, nine cycles (I to IX) of marly limestones alternating with marls are observed.  
40x65mm (300 x 300 DPI)

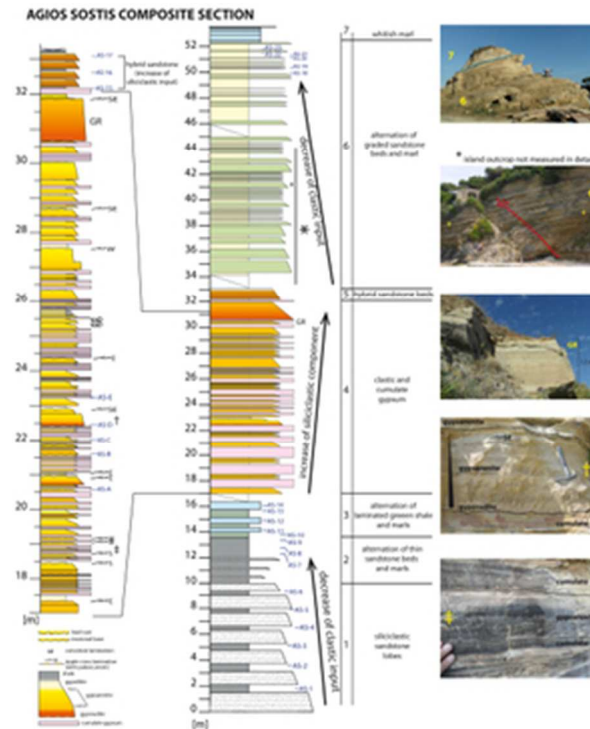


Fig. 7. Agios Sostis composite section: lithology, samples location, and facies characteristics of the different stratigraphic levels.  
12x15mm (600 x 600 DPI)



Fig. 8. Sedimentary facies details of the PLG and RLG units. Argassi area: a. selenite, b. branching selenite. Agios Sostis area: c. pre-evaporitic sequence and MES boundary with the overlying RLG unit, d. gypsum turbidites, e: convolute lamination, f: alternations of primary cumulate gypsum (CU) and clastic gypsarenite (AR) and gypsrudite (GR). 23x26mm (300 x 300 DPI)

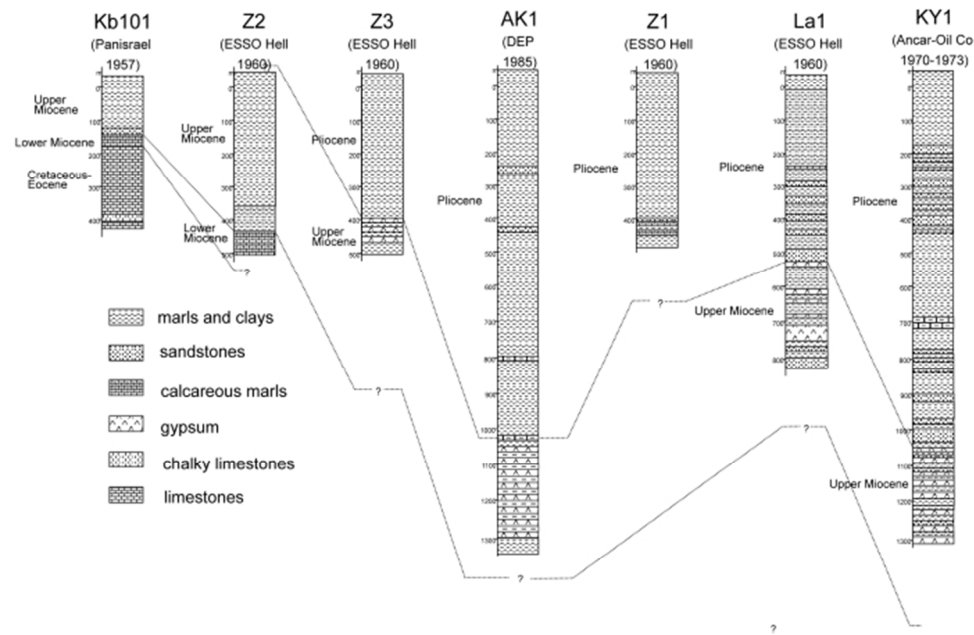


Fig. 9. Zakynthos (Alikanas) basin wells positioned in a west-to-east direction (the wells' locations are indicated in fig. 1). Correlation of the borehole logs shows that the Neogene deposits (gypsum included) increase their thickness eastward. Agios Kyrikos-1 well (AK-1) revealed indirect indices of halite accumulation in the Messinian gypsum stratigraphic level.

60x40mm (300 x 300 DPI)

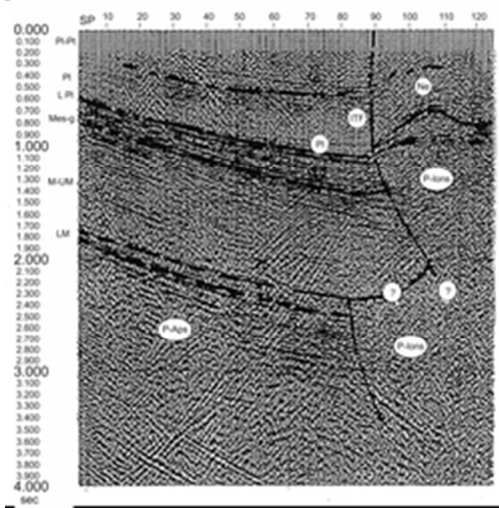


Fig. 10. Alikanas basin seismic profile (modified from the initial representation by Marinescu; in Nikolaou, 1986). The seismic profile shows a) the position of the Ionian thrust, b) the eastward increase in the thickness of the Neogene deposits. The seismic line's location is indicated in Fig. 1. PL-PT: Pliocene-Pleistocene, PI: Pliocene, LPI: lower Pliocene, Mes-g: Messinian gypsum, M-UM: middle-upper Miocene, LM: lower Miocene, P-Aps: pre-Neogene sequence of the Pre-Apulia zone, P-Ions: pre-Neogene sequence of the Ionian zone (Triassic evaporites), ITF: Ionian thrust front, Ne: undifferentiated Neogene, SP: shot point, sec: time in seconds.  
20x21mm (300 x 300 DPI)

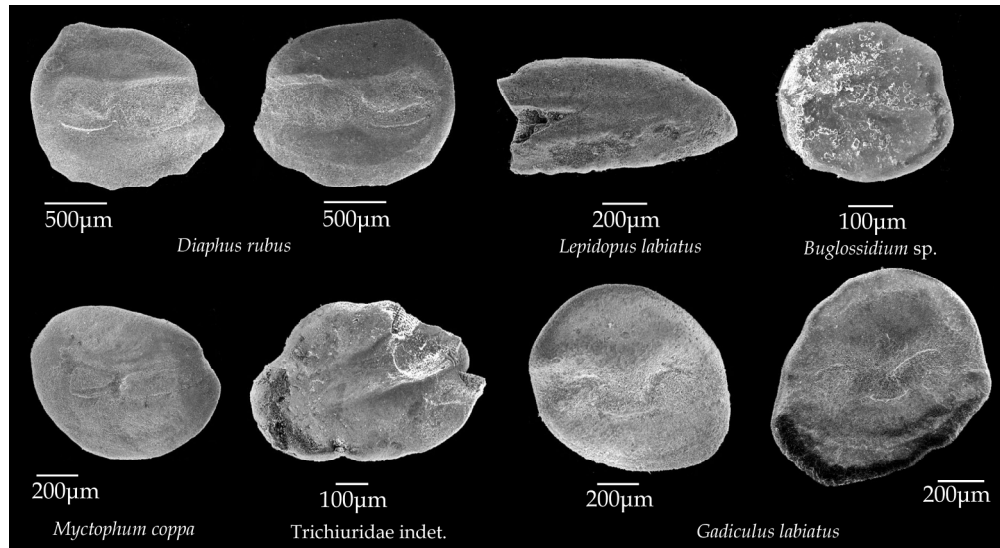


Fig. 11. Fish otoliths discovered in the pre-evaporitic sequence of Kalamaki section.  
187x101mm (300 x 300 DPI)

Unable to Convert Image

The dimensions of this image (in pixels) are too large to be converted. For this image to convert, the total number of pixels (height x width) must be less than 40,000,000 (40 megapixels).

Fig. 12. A: plots of VGP latitude of the West and East Kalamaki subsections. B: plots of ChRM directions corrected for bed tilting, full and empty red and purple circles represent normal and reversed mean direction for Kalamaki West and east subsection, respectively. C: Zijderveld diagrams with demagnetization paths of selected samples from the Kalamaki west subsection.

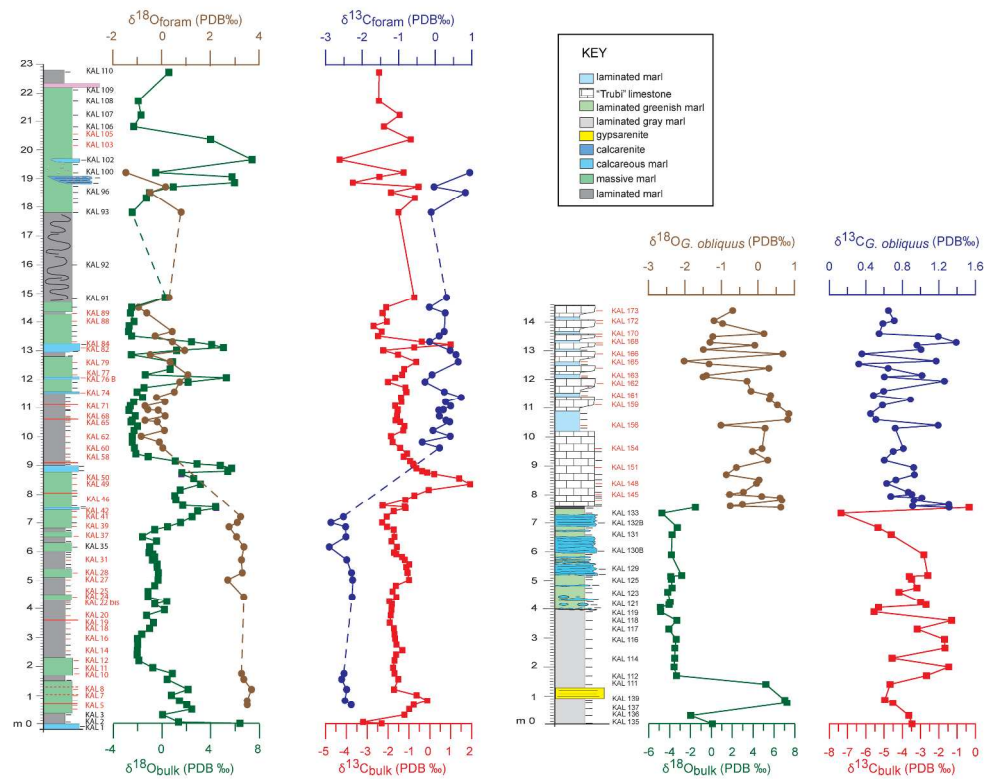


Fig. 13. Pre-evaporitic sequence, Lago-Mare, and Trubi Formation carbon and oxygen stable isotopes. 278x223mm (300 x 300 DPI)



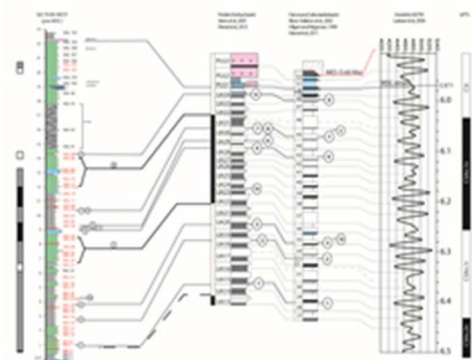


Fig. 14. Chrostratigraphic framework of Kalamaki section's pre-evaporitic sequence and correlation with Perales section (Sorbas basin) (modified after Sierro et al., 2001; Manzi et al., 2013) and Falconara section (Caltanissetta basin) (modified after Blanc-Valleron et al., 2002; Hilgen & Krijgsman, 1999; Manzi et al., 2011) via the astronomical Insolation summer curve of Laskar et al. 2004 and GPTS of Lourens et al., 2004. Bio-magnetostratigraphic events are: 1) FAO T. multiloba; 2) FAO dextral N. acostaensis; 3) G. scitula influx; 4) N. acostaensis dominance sinistral; 5) T. multiloba influx; 6) G. scitula influx; 7) dominance N. acostaensis sinistral; 8) Last abundant influx T. multiloba; 9) HO planktonic Foraminifera; I) top C3An.1n; II) boundary C3An.2n/C3r.

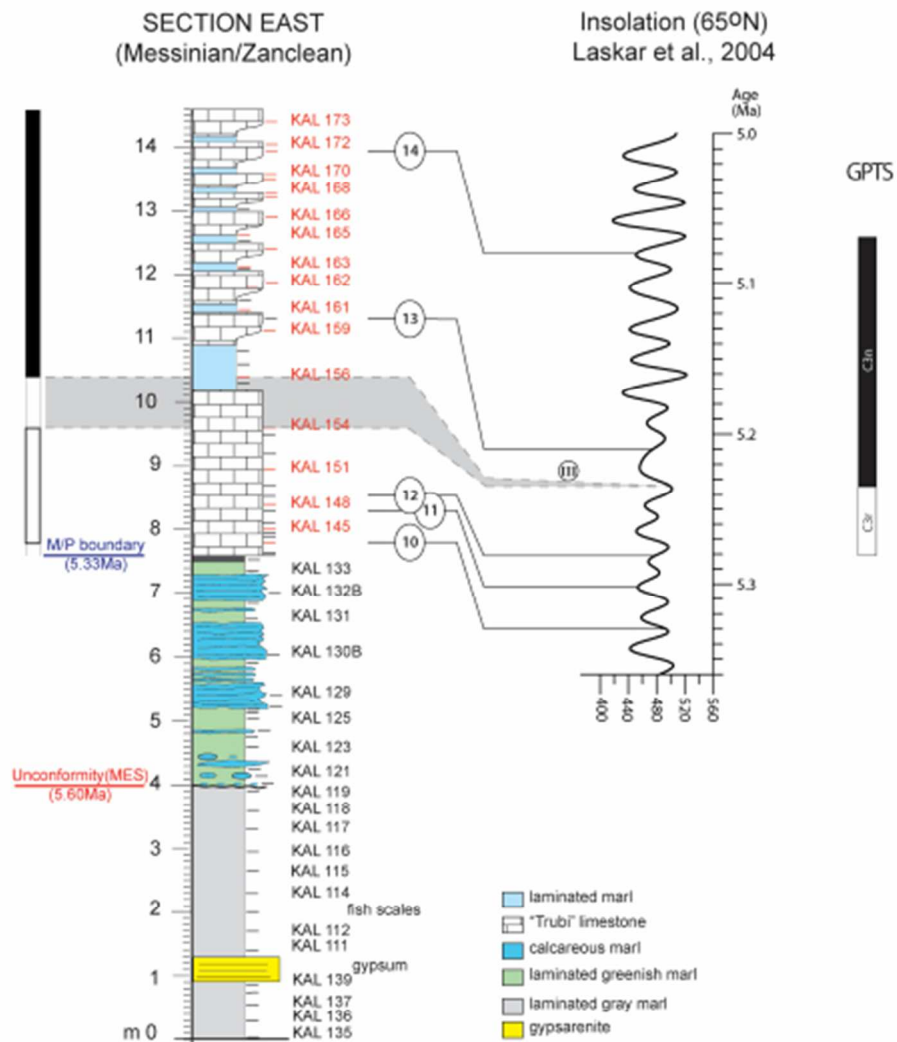


Fig. 15. Kalamaki section age model of the PLG top portion, Lago-Mare, and Trubi Formation, correlated with insolation curve (based on Laskar et al., 2004).  
40x48mm (300 x 300 DPI)

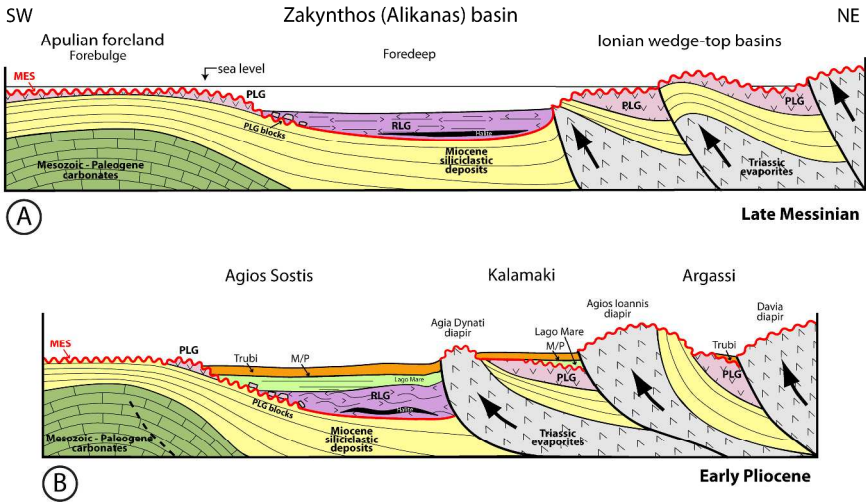


Fig. 16. Paleogeographic reconstruction.

A. During the Messinian, the Zakynthos (Alikanas) foreland basin was formed in front of the Ionian thrust. The Neogene formations deposited over the Pre-Apulian domain corresponded to the foredeep and the flank between foredeep and forebulge, whereas those overlying the Ionian zone corresponded to the wedge-top, which was uplifted due to the diapiric movements of the Ionian Triassic evaporites. In the 1st MSC stage, PLG was deposited on both forebulge and wedge-top. In the 2nd MSC stage, PLG was totally or partially eroded (creating the Messinian Erosional Surface; MES) and redeposited with correlative conformity mainly as gypsum turbidites (RLG unit) in the depocenter of the foreland basin.

B. During the end of the Messinian, in Kalamaki-Argassi wedge-top area the Lago-Mare sediments were unconformably overlying the Primary Lower Gypsum above the MES, while in the depocenter of the foreland basin they were conformably deposited over the Resedimented Lower Gypsum. The Zanclean flood was recorded on both areas by the conformable deposition of the Trubi Formation.

With red raffled and continuous line the unconformity and the correlative conformity of the MES, respectively.

316x189mm (300 x 300 DPI)

Family	Genus/Species	Ecology	References
Gonostomatidae	indet.	-	-
Sternoptychidae	<i>Maurolicus muelleri</i> (Gmelin, 1789)	0-1524 m, usually 300-400 m; SP-Tr; marine, bathypelagic	Mauchline, 1988; Wheeler, 1992
Phosichthyidae	<i>Vinciguerrria poweriae</i> (Cocco, 1838)	50-1000 m, usually 300-600 m; ST-Tr; marine, bathypelagic	Mundy, 2005
Myctophidae	<i>Ceratoscopelus maderensis</i> (Lowe, 1839)	51-1082 m; Te; marine, bathypelagic	Hulley, 1990; Mytilineou <i>et al.</i> , 2005
	<i>Diaphus cavallonis</i> Brzobohaty and Nolf, 2000 *	-	-
	<i>Diaphus cf. pedemontanus</i> Robba, 1970 *	-	-
	<i>Diaphus rafinesquii</i> (Cocco, 1838)	40-1200 m; Te; marine, bathypelagic	Hulley, 1990
	<i>Diaphus rubus</i> Girone et al., 2010 *	-	-
	<i>Diaphus taaningi</i> Norman, 1930	40-475 m; Tr; marine, bathypelagic	Hulley, 1990
	<i>Myctophum coppa</i> Girone et al., 2010 *	-	-
Moridae	<i>Physiculus</i> aff. <i>huloti</i> Polli, 1953	92-320 m; Tr; marine, benthopelag.	OBIS, 2006
Gadidae	<i>Gadiculus argenteus</i> Guichenot, 1850	100-1000 m; Te-ST; marine, pelagic- oceanic	Muus & Nielsen, 1999
	<i>Gadiculus labiatus</i> (Schubert, 1905) *	-	-
Gobiidae	indet.	-	-
Trichiuridae	<i>Lepidopus caudatus</i> (Euphrasen, 1788)	42-620 m, usually 100-300 m; ST-Te	Mytilineou <i>et al.</i> , 2005
Soleidae	<i>Buglossidium</i> sp.	5-450 m, usually 10- 40 m; ST	Muus & Nielsen, 1999